Cellulose (2025) 32:9085–9110
https://doi.org/10.1007/s10570-025-06752-z

ORIGINAL RESEARCH

Comparative study of the bioactivities of *Mesembryanthemum crystallinum* polysaccharides and their corresponding Co–CuO–Ag trimetallic nanoparticles

Hussein H. Hammam · E. M. Khalil · Ahmed H. I. Faraag · Salim Mohamed Abd El-Aziz

Received: 23 February 2025 / Accepted: 21 August 2025 / Published online: 8 September 2025
© The Author(s) 2025

Abstract This study employs polysaccharides (PS) extracted from *Mesembryanthemum crystallinum* (*M. crystallinum*) as a safe and bio-compatible medium for the synthesis of cobalt (CoNPs), copper oxide (CuONPs), silver (AgNPs), and trimetallic nanoparticles (TMNPs). The nanoparticle synthesis was optimized using UV–visible spectroscopy to determine the optimal conditions, which were found to be 60 °C, a pH of 13, and a reaction time of 60 min. Scanning Electron Microscopy (SEM) confirmed the deposition of nanosized CoNPs, CuONPs, AgNPs, and TMNPs onto a cotton fabric surface, while Transmission Electron Microscopy (TEM) revealed their spherical morphology with particle size 5–20 nm. In vitro anticancer analyses were performed on breast cancer (MCF-7), human liver cancer (HEPG-2), and normal lung (WI-38) cell lines, the cytotoxic activity of TMNPs was found to be the highest for MCF-7 with a concentration of 14.7 µg/ mL. For HEPG-2, TMNPs recorded highest activity 17.81 µg/ mL, followed by CoNPs 30.53 µg/ mL, CuONPs recorded 33.7 µg/ mL, AgNPs recorded 42.6 µg/ mL, PS recorded 55.98 µg/Ml. Moreover, TMNPs showed enhanced anti-inflammatory activity with Oedema inhibition rates of 87.04% compared to 80.25%, 74.07%, 66.05%, and 56.79% for CuONPs, CoNPs, AgNPs, and polysaccharides, respectively. A wound healing study indicated that TMNPs produced maximum wound area reductions of 85.11%, followed by 79.72% after ten washes. These results underscore *M. crystallinum* polysaccharides as eco-friendly agents, advancing further innovative biomedical nanotechnology applications.

Keywords *Mesembryanthemum crystallinum* · Polysaccharides · Anti-inflammatory · Wound healing

Abbreviations

AgNPs	Silver nanoparticles
TMNPs	Trimetallic nanoparticles
CoNPs	Cobalt nanoparticles
CuONPs	Copper oxide nanoparticles
DPPH	2,2-Diphenyl-1-picrylhydrazyl (a free radical used in antioxidant assays)
FTIR	Fourier-transform infrared spectroscopy
HEPG-2	Human liver cancer cell line
HPLC	High-performance liquid chromatography
IC_{50}	Half-maximal inhibitory concentration
MCF-7	Human breast cancer cell line

Supplementary Information The online version contains supplementary material available at https://doi.org/10.1007/s10570-025-06752-z.

H. H. Hammam · E. M. Khalil · S. M. A. El-Aziz (✉)
Chemistry Department, Faculty of Science, Helwan University, Ain-Helwan, Cairo 11795, Egypt
e-mail: SMabdelaziz@science.helwan.edu.eg

A. H. I. Faraag
School of Biotechnology, Badr University in Cairo, Badr City, Cairo 11829, Egypt

MTT	3-(4,5-Dimethylthiazol-2-yl)-2,5-diphenyltetrazolium bromide (a cell viability assay)
NPs	Nanoparticles
PS	Polysaccharides
SEM	Scanning electron microscopy
TEM	Transmission electron microscopy
UV–Vis	Ultraviolet–visible spectroscopy
WI-38	Normal human lung fibroblast cell line
XRD	X-ray diffraction
EDX	Energy dispersive X-ray

Introduction

Mesembryanthemum crystallinum, a creeping succulent in the Aizoaceae family, originated in Africa, Sinai, and southern Europe and has since disseminated to North America, South America, and Australia (Bouftira et al. 2008; Kang and Joo 2023). In response to osmotic challenges such as drought and salinity, this plant accumulates protective solutes, including polysaccharides, amino acids, polyols, betaines, and ectoines, in its cytoplasmic compartments (Bohnert and Shen 1998).

M. crystallinum, commonly referred to as the ice plant, is a salt-tolerant species known for its diverse medicinal benefits and potential uses in agriculture. This plant is rich in polyphenols, especially flavonoids like apigenin and luteolin, which contribute to its strong antioxidant properties (Calvo et al. 2022; Kang and Joo 2023). It also exhibits antihypertensive and hypoglycemic effects by inhibiting certain enzymes (Calvo et al. 2022). The ice plant's anti-inflammatory capabilities are demonstrated by its reduction of inflammatory cytokines and nitric oxide production (Kang and Joo 2023). Various parts of the plant contain differing amounts of bioactive compounds and exhibit distinct activities (Kang and Joo 2023). The plant's ability to transition from C3 to CAM photosynthesis under stress increases its salt tolerance, making it a promising candidate for cultivation in saline soils (Loconsole et al. 2019). Moreover, its potential for phytoremediation of polluted water and soil is attracting growing research attention (Yapias 2024). *M. crystallinum*, a salt-tolerant plant with a history of medicinal use, has exhibited notable antioxidant and antimicrobial activities. Methanolic extracts from this plant have shown strong antioxidant effects when evaluated with the DPPH assay and have demonstrated broad-spectrum antibacterial activity against both gram-positive and gram-negative bacteria (Ibtissem et al. 2012). The medicinal benefits are largely due to the polyphenolic compounds present in the extracts. Moreover, certain extracts from the Chrysanthemum genus have been found to have activity against HSV-1 (Vasas et al. 2015).

The polysaccharide extract of *M. crystallinum* had a positive effect on scavenging hydroxyl radicals, 1,1-diphenyl-2-trinitrophenyl hydrazine (DPPH), and nitrite ions. The potential of *M. crystallinum* polysaccharide extract to serve as an antioxidant on animal oil and vegetable oil was found to have a positive correlation with the concentration within a certain addition range. In addition, the polysaccharide of *M. crystallinum* showed antibacterial activity against *Escherichia coli* and *Bacillus subtilis*.

Choosing *M. crystallinum* for nanoparticle synthesis is influenced by multiple factors. Its abundance of bioactive compounds, particularly antioxidants, makes it an excellent choice for eco-friendly nanoparticle production. These compounds help in reducing metal ions and stabilizing nanoparticles, offering a sustainable alternative to conventional chemical methods. Moreover, the plant's adaptability to various environmental conditions and widespread availability make it a practical and sustainable resource for nanoparticle creation. The potential uses of nanoparticles derived from *M. crystallinum* in areas like drug delivery, antimicrobial treatments, and sensor technology underscore the plant's substantial importance in nanotechnology research (Yedoti and Supraja 2024).

Polysaccharides are complex carbohydrates composed of long chains of monosaccharide units connected via glycosidic linkages (Aachary and Prapulla 2011; Delattre et al. 2011). Found ubiquitously across all domains of life, these biopolymers exist in algae (e.g., alginate), terrestrial plants e.g., starch and cellulose (Rinaudo et al. 2014), and microorganisms e.g., zymosan and dextran (Domingues et al. 2022; He et al. 2022; Gomez-Hermoso-de-Mendoza et al. 2023; Tang et al. 2024; Schiavi et al. 2024; Aouay et al. 2024). Due to their bioactive nature, polysaccharides extracted from medicinal plants and mushrooms exert a diverse array of pharmacological effects, including antioxidants, immunomodulatory, anticancer, gastrointestinal protective, antidiabetic, and hepatoprotective properties (Xie et al. 2016; Raji

et al. 2023; Al-darwesh et al. 2025a, b; Ibrahim et al. 2025).

In the field of nanotechnology, a wide range of enhanced properties, such as increased catalytic activity, improved antimicrobial efficacy, multifaceted morphology, heightened detection sensitivity, advanced drug encapsulation performance, greater bioavailability, and efficient chemical transformation—have been demonstrated for bimetallic (BMNPs) and trimetallic nanoparticles (TMNPs), particularly when compared to their monometallic counterparts (Li et al. 2018; Pandey and Pandey 2016; Masud et al. 2023). Metal nanoparticles including silver (Ag), gold (Au), cobalt (Co), palladium (Pd), platinum (Pt), and copper oxide (CuO) are highly sought after within both therapeutic and consumer sectors (Aouay et al. 2024; Shafqat et al. 2025). Silver nanoparticles (AgNPs), for instance, are prominently produced with an annual capacity of approximately 500 tonnes and are employed in anti-infective, anti-angiogenic, and antibacterial applications (Almatroudi et al. 2020; Irfan et al. 2021; Jan et al. 2021; Allemailem et al. 2022a, b; Irfan et al. 2022; Awais et al. 2023; Rehan et al. 2024; Al-darwesh et al. 2024a; Bhavi et al. 2024a, b, c; Ihsan et al. 2024).

Cobalt nanoparticles (CoNPs) have attracted considerable attention. Owing to their diverse and unique applications. These nanoparticles exhibit multifunctional properties that render suitable for biomedical applications (e.g., antimicrobial, antiviral, antileishmanial, targeted therapies, anticancer, and drug delivery), as well as for use in chemical sensors, solar selective absorbent materials, electrode materials in rechargeable batteries, dyes, and electronic thin films (Waris et al. 2021; Al-darwesh et al. 2024b, c) . Their magnetic, electrical, and catalytic characteristics facilitate applications in magnetic recording devices, biosensors, magnetohydrodynamics (MHD), magnetic fluids, composites, and catalysts (Puntes et al. 2001; Ansari et al. 2017) demonstrated the synthesis of CoNPs via a one-step hydrothermal method using oleic acid as a capping agent, and subsequently examined their essential structural, physical, magnetic, and chemical properties.

Similarly, copper oxide nanoparticles (CuONPs) are considered promising alternatives for numerous natural and industrial applications, due to their abundance, low toxicity, small bandgap, and cost-effectiveness. The advantageous biological applications of CuONPs have been corroborated through in vitro cytotoxicity studies using traditional mammalian cell cultures, organoid models, and vascular plant cell systems (Narayana et al. 2024; Kir et al. 2024; Parveen and Riazunnisa, 2025).

To date, the biomedical synthesis of CoNPs, CuONPs, AgNPs, and TMNPs using polysaccharides derived from *M. crystallinum* has not been reported. Therefore, the present study aims to biosynthesize these nanoparticles using *M. crystallinum* polysaccharides and to comprehensively assess their synergistic anticancer, wound healing, and anti-inflammatory properties.

Materials and methods

Collection of M. crystallinum plant

M. crystallinum leaves were harvested from the Behera Governorate in Egypt. The samples were meticulously rinsed using running tap water to eliminate any particulate matter, then dried in the shade to preserve their biochemical integrity. The plant identification was verified by a taxonomist. The added text specifies that the specimen of *M. crystallinum* was authenticated by **Dr. Emad Farahat** (Professor in Botany) at the **Helwan University Herbarium of Botanical Sciences**, and that a voucher specimen has been deposited under the voucher number **HUHBS-2023-007**. Subsequently, the leaves were arranged on an oven tray and subjected to controlled drying at temperatures ranging from 30 to 40 °C overnight. Once the samples were completely dehydrated, they were finely powdered using a suitable milling process and subsequently stored in airtight containers until further extraction procedures were performed.

Extraction of polysaccharides

The first step in the process was subjecting a 50 g sample of *M. crystallinum* plant material to repeated water percolation, which was then followed by complete extraction using a reflux system until the extraction was performed completely. Using a rotary evaporator, the extract that was produced was concentrated to a volume of around sixty milliliters. The polysaccharides (PS) were then precipitated using absolute

ethanol, and the residue of the PS was washed with absolute ethanol after it had been precipitated. After that, the residue was weighed and stored for further examination.

Hydrolysis of the polysaccharides for HPLC analysis

In a boiling water bath, 0.1 g of M. crystallinum phytosubstance (PS) was added to 10 mL of 2 N HCl and maintained for 5 h to ensure complete hydrolysis. The resulting hydrolysate was treated with $Ba(OH)_2$. After the solution was evaporated to a final volume of 2 mL, it was centrifuged and washed with water. After that, it was partitioned three times with ethyl acetate and then injected into an HPLC system (Abd El-Aziz and Farahat 2023).

Synthesis of AgNPs

A 0.05 g of dried *M. crystallinum* polysaccharide (PS) was dissolved in 100 mL of distilled water using a heating magnetic stirrer. To optimize the synthesis of silver nanoparticles (AgNPs), 1 mL of (0.1 M) $AgNO_3$ was added to the PS extract. The ratio of the precursor solution to the PS extract is 1:5. The resulting reaction mixture underwent continuous stirring under varying conditions, specifically at temperatures of 40 °C, 50 °C, 60 °C, and 70 °C; durations of 15 min, 30 min, 45 min, and 60 min; and at pH values of 11, 12, and 13.

Synthesis of CuONPs

After dissolving 0.1 g of PS in 100 mL of distilled water, 2 mL of 0.1 M copper sulfate heptahydrate was added to the solution. The reaction mixture was then maintained under variable conditions to determine the optimum parameters for copper oxide nanoparticle (CuONP) synthesis. Specifically, the mixture was subjected to temperatures of 40 °C, 50 °C, 60 °C, and 70 °C for durations of 15 min, 30 min, 45 min, and 60 min, respectively, and at pH values of 11, 12, and 13.

Synthesis of CoNPs

An aqueous solution of cobaltous nitrate hexahydrate was employed in conjunction with a polysaccharide extract derived from *M. crystallinum* for the synthesis of cobalt nanoparticles (CoNPs). The polysaccharide extract was prepared by dissolving 0.05 g of the dry sample in 100 mL of distilled water. Subsequently, a 0.5 mL of a 0.1 M cobaltous nitrate hexahydrate solution was added to the extract. The resulting reaction mixture was maintained under varying conditions, with temperatures ranging from 40 to 70°C, reaction times from 15 to 60 min, and pH levels between 10 and 13, determining the optimal parameters for CoNPs synthesis.

Synthesis of trimetallic nanoparticles (TMNPs)

The polysaccharide extract was prepared by dissolving 0.3 g of dry PS in 100 mL of distilled water. Subsequently, equal volumes (1:1:1) of 0.1 M silver nitrate ($AgNO_3$), 0.1 M copper sulfate heptahydrate, and 0.05 M cobalt nitrate hexahydrate $(Co(NO_3)_2 \cdot 6H_2O)$ solutions were added to the extract. The resulting reaction mixture was then continuously stirred at various temperatures (40 °C, 50 °C, 60 °C, and 70 °C) to determine the optimal synthesis conditions (Abd El-Aziz and Farahat 2023).

Characterization techniques

The observed color change confirmed the synthesis of AgNPs, CuONPs, CoNPs, and TMNPs. Specifically, the formation of these nanoparticles was verified through UV–visible spectroscopy, which was conducted using a Jasco UV–Vis spectrophotometer (Model V-670, double beam) with the polysaccharide extract serving as the blank. After synthesis, the nanoparticles were dried at 50 °C. The dried nanoparticles were subsequently characterized using Fourier-transform infrared (FTIR) spectroscopy with a Nicolet 870 system (El-Rafie et al. 2016a, b). X-ray diffraction (XRD) analysis was then carried out using a Shimadzu 6000 instrument (Japan) to further analyze the nanoparticles (El-Sayyad et al. 2022; Abou Hussein et al. 2021). The size, distribution, and morphology of the nanoparticles were determined by transmission electron microscopy (TEM) using a JEOL JEM 2100 instrument (Japan) (El-Rafie et al. 2023). Furthermore, the presence of nanosized CoNPs, CuONPs, AgNPs, and TMNPs on the surface of cotton fabric was confirmed by scanning electron microscopy (SEM, model JXA-840A; Japan) (El-Sayyad et al.

2022). The elemental composition was detected using Zeiss Smart EDX (Lakshmi et al. 2019).

Anticancer activity

Treatment of cell lines

Nanoparticle solutions were dissolved in DMSO (99%) to achieve the desired concentrations. Subsequently, MCF-7, HEPG-2, and WI-38 cells (5,000 cells per well) were seeded in 96-well flat-bottom microplates and allowed to adhere for 24 h. Following this initial incubation, the cells were exposed to five different concentrations of nanoparticles, prepared via tenfold serial dilutions, 48 h after seeding. The concentrations applied were 100 µg/mL, 50 µg/mL, 25 µg/mL, 12.5 µg/mL, and 6.5 µg/mL, with control wells receiving only the growth medium. After treatment with the nanoparticle doses for an additional 48 h, Doxorubicin was used as a positive control.

MTT assay

Cell viability was determined using the MTT assay 72 h after the addition of nanoparticles. In this essay, each well received 50 µL of an MTT solution (5 mg/mL) prepared in phosphate-buffered saline (PBS). The microplates were then incubated for an additional 4 h to allow viable cells to reduce MTT to the insoluble purple formazan product, whereas nonviable cells maintained the yellow coloration. Following incubation, 100 µL of dimethyl sulfoxide (DMSO) was added to dissolve the formazan crystals. The absorbance of the blank was subtracted from the absorbance of the corresponding sample containing the target cells. The half-maximal inhibitory concentration (IC_{50}), defined as the concentration required to achieve a 50% reduction in cell viability compared to the vehicle-treated control, this effect has been widely studied) Riss et al. 2016; Carreño et al. 2021).

Wound healing and anti-inflammatory

Treatment of Fabrics with NPs

Cotton fabrics were immersed in a 2% solution of mono and TMNPs to achieve a 100% wet pick-up. The fabrics were then dried for 3 min at 80 °C, followed by a curing process of 3 min at 140 °C. Subsequently, the nanoparticle-treated fabric samples were examined by scanning electron microscopy (SEM) to assess surface morphology and nanoparticle distribution.

Material

El-Mahalla Company graciously provided cotton fabrics for weaving and spinning applications. Carrageenan was obtained from Sigma–Aldrich (USA), Persil detergent was supplied by Henkel (Egypt), and Silver Sulphadiazine ointment (S.S. Oint cream) was procured from Kahira Pharm. Ind. Co. (ARE).

Washing the finished fabrics

The fabrics, which were treated with various nanoparticles, underwent 10 washing cycles. The washing procedure involved submerging the samples in 100 mL of a 3% v/v aqueous detergent solution at a temperature of 49 ± 2 °C.

Method

Thirty-six albino rats were randomly allocated into six groups ($n = 6$ per group): The Blank Control Group (1): Rats received a blank cotton film, serving as the negative control without any active agent. AgNPs Group (2): Rats were treated with cotton fabrics coated with AgNPs that had endured 10 washing cycles. CuONPs Group (3): Rats were treated with cotton fabrics coated with CuONPs that had undergone 10 washing cycles. CoNPs Group (4): Rats were treated with cotton fabrics coated with CoNPs that had completed 10 washing cycles. TMNPs Group (5): Rats received cotton fabrics treated with TMNPs that had been washed 10 times. Drug Standard Group (6): Rats were administered Silver Sulphadiazine ointment (S.S. Oint) as the positive control to validate the anti-inflammatory efficacy. Each film was secured firmly to the dorsal skin of the animals. After an acclimatization period of one- hour post-application, each animal received a subplantar injection of 0.1% carrageenan solution in saline (0.1 mL) in the right hind paw, designed to induce an inflammatory response. In contrast, the left hind paw was injected with 0.1 mL of saline alone, functioning as an internal control to

differentiate the inflammatory effects of carrageenan from those due solely to the injection procedure. The rats were sacrificed for 4 h following film application. At predetermined intervals (two, three-, and four-hour post-injection), both hind paws were excised and subsequently weighed to quantify the degree of Oedema, thereby providing a measure of the inflammatory response (Alaa et al. 2016).

Control group justification

The blank control group (1) provided a baseline to assess any inherent anti-inflammatory effects of the cotton film without nanoparticle treatment. This is critical for distinguishing the actions of the active agents (nanoparticles) from any potential effects of the fabric substrate. The Drug Standard Group (6) served as a positive control. Using silver sulfadiazine ointment, which is a well-known anti-inflammatory medicine, helped us compare how well the nanoparticle treatments worked. This group validated the experimental model by confirming that a known therapeutic agent could mitigate the inflammatory response. Additionally, the saline injection in the left hind paw served as an intrinsic control for the injection protocol, ensuring that any observed inflammation in the right hind paw was attributable specifically to carrageenan-induced inflammation rather than procedural artifacts. This comprehensive experimental design enables a robust comparison between the nanoparticle treatments and established controls, thereby substantiating the anti-inflammatory potential of the nanoparticle-coated fabrics.

Experimental animals

Male Sprague–Dawley rats, weighing between 140 and 160 g, were acquired from the animal facility at the National Research Center in Cairo, Egypt. The subjects were maintained under uniform hygienic conditions and were provided with a standard laboratory diet to ensure consistency in nutritional intake throughout the experimental period.

Experimental design

Following the induction of the wound, the experimental subjects were subsequently allocated into six distinct groups (Groups 1–6) as delineated in the previous section.

Wound creation

Wound contraction was evaluated using an excision wound model in accordance with previous studies (El-Rafie et al. 2016a, b; El-Rafie et al. 2022). Full-thickness skin lesions were created on the dorsal interscapular region of rats. The animals were anesthetized with ether, and their dorsal fur was removed using electric clippers via an open mask method. Incisions were made by excising approximately 2 cm^2 of skin from the shaved area, after which an appropriate dressing was applied to each wound. The dressings were replaced daily, and at each dressing change the wounds were examined, photographed, and measured. Wound healing was quantified as the wound area in mm^2, and wound contraction was assessed as the percentage reduction from the initial wound dimensions.

$$\%\ \text{Reduction} = \frac{(\text{Wound area on day } 0 - \text{Wound area on day } n)}{\text{Wound area on day } 0} \times 100 \quad (1)$$

Complete epithelialization is defined as the stage at which the scab completely detaches, leaving no residual wound tissue. The duration required to achieve this endpoint is recorded as the period of epithelialization.

Statistical analysis

The results were presented from six animals in each group as a mean value with its standard deviation (mean ± SE).

Results and discussions

HPLC analysis of the polysaccharide hydrolysates

High-performance liquid chromatography (HPLC) analysis of the hydrolysates obtained from the water extracts of *M. crystallinum* polysaccharides demonstrated that 5 sugars constituted 89.250% of the overall composition. Among these, the predominant sugars were glucose (38.07%), galactose (30.21%), and xylose (7.09%) (Table 1).

Table 1 Identified monosaccharides in *M. crystallinum* PS hydrolysate

Authentic sugars	RT	Relative %
Glucose	10.45	38.07
Galactose	11.13	30.21
Rhamnose	7.98	5.35
Xylose	8.17	7.09
Mannose	10.76	5.34
Total identified sugars	89.25	
Unidentified sugars	10.75	

Structural analyses of the prepared nanoparticles and TMNPs

UV–Vis spectroscopy

AgNPs, CuONPs, CoNPs, and TMNPs were characterized by recording the UV–Vis absorption spectra of the reaction mixtures. UV–Vis spectroscopy served as an essential technique for confirming the formation and stabilization of the synthesized nanoparticles in aqueous solutions. To optimize the synthesis process, the reaction mixture was incubated under various conditions including temperatures (40–70 °C), durations (15–60 min), and pH values (10–13)—to determine the optimal parameters. The absorption peaks for AgNPs, CuONPs, and CoNPs were observed at approximately 400–450 nm, 220–250 nm, and 210–260 nm, respectively, whereas TMNPs exhibited two distinct absorption peaks at 210–240 nm and 400–445 nm as illustrated in Figs. 1, 2 and 3 (Al-Marhaby and Seoudi 2016; Al-Haddad et al. 2020; Khani and Irani 2020; Chakraborty et al. 2022; Abbigeri et al. 2024; Singh et al. 2025).

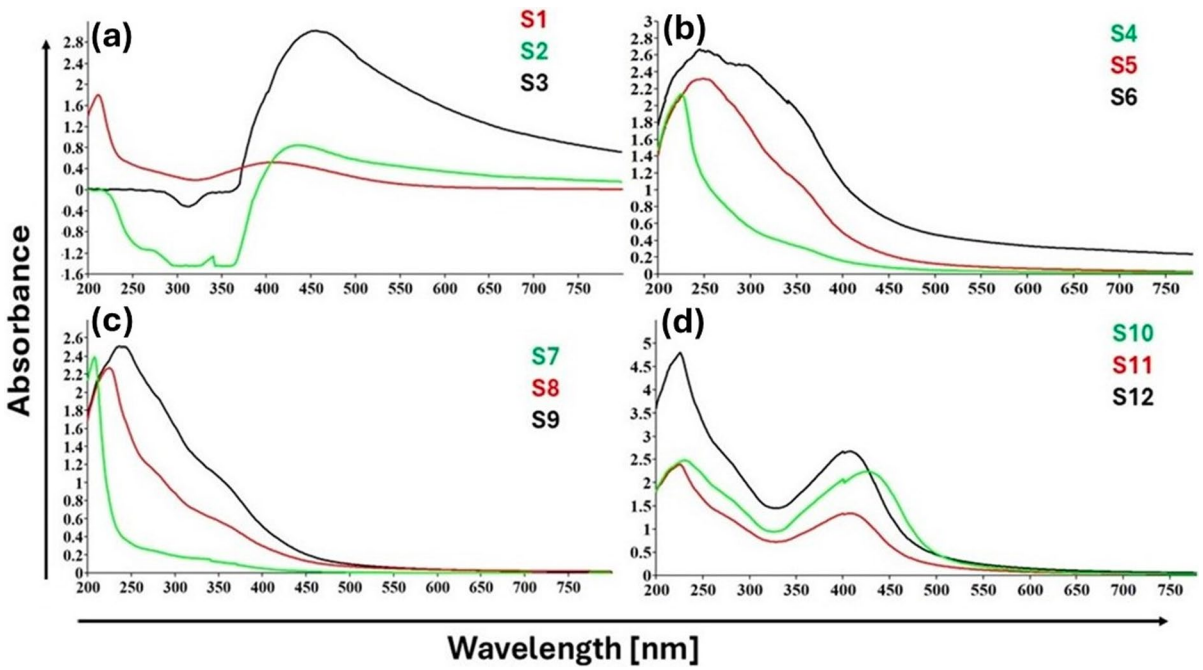


Fig. 1 UV–visible absorption peaks of **a** AgNPs, **b** CuONPs, **c** CoNPs, and **d** TMNPs at different pH, constant temperature and time

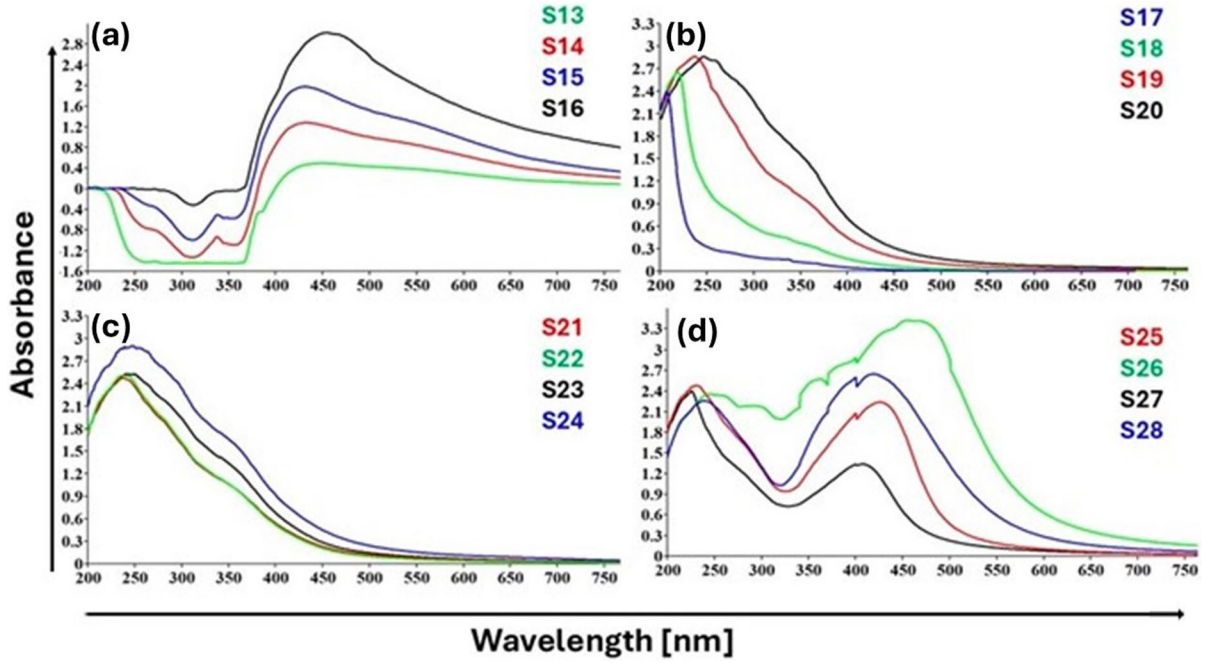


Fig. 2 UV–visible absorption peaks of **a** AgNPs, **b** CuONPs, **c** CoNPs, and **d** TMNPs at different temperatures constant pH, and time

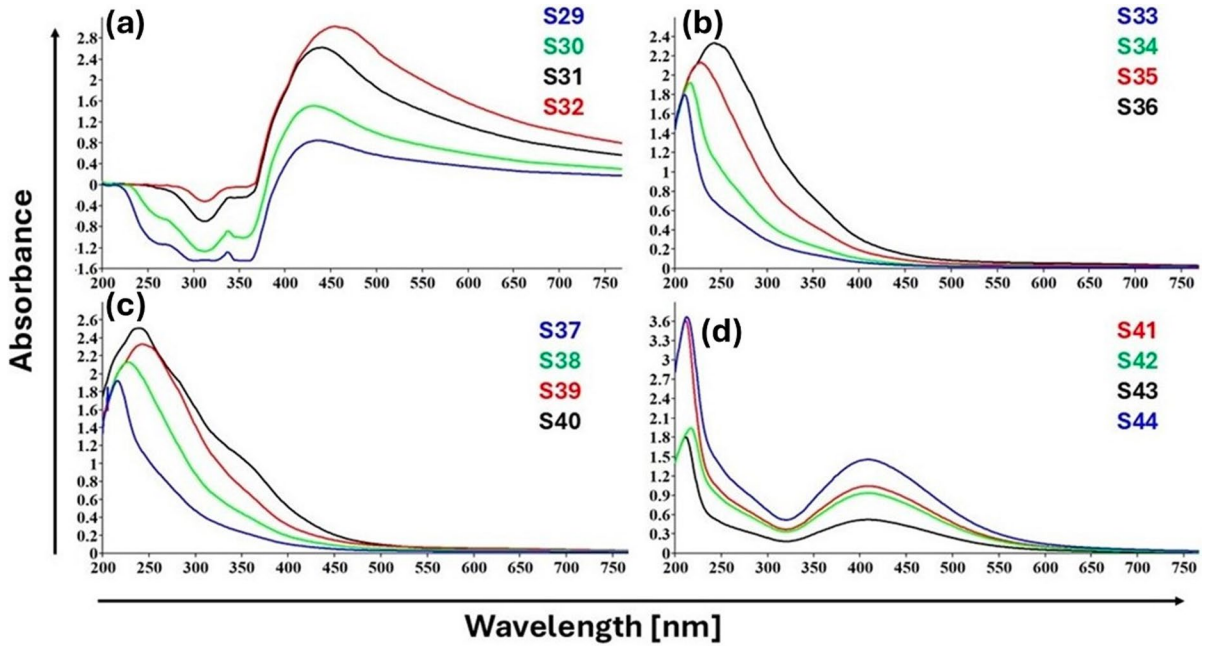


Fig. 3 UV–visible absorption peak of **a** AgNPs, **b** CuONPs, **c** CoNPs, and **d** TMNPs at different time constant pH, and temperature

Table 2 Samples description

Sample	pH	Temp. (°C)	Time(min)	Identification
Effect of pH				
S1	11	60	45	AgNPs
S2	12	60	45	AgNPs
S3	13	60	45	AgNPs
S4	11	60	45	CuONPs
S5	12	60	45	CuONPs
S6	13	60	45	CuONPs
S7	11	60	45	CoNPs
S8	12	60	45	CoNPs
S9	13	60	45	CoNPs
S10	11	60	45	TMNPs
S11	12	60	45	TMNPs
S12	13	60	45	TMNPs
Effect of temperature				
S13	13	40	60	AgNPs
S14	13	50	60	AgNPs
S15	13	60	60	AgNPs
S16	13	70	60	AgNPs
S17	13	40	60	CuONPs
S18	13	50	60	CuONPs
S19	13	60	60	CuONPs
S20	13	70	60	CuONPs
S21	13	40	60	CoNPs
S22	13	50	60	CoNPs
S23	13	60	60	CoNPs
S24	13	70	60	CoNPs
S25	13	40	60	TMNPs
S26	13	50	60	TMNPs
S27	13	60	60	TMNPs
S28	13	70	60	TMNPs
Effect of time				
S29	13	60	15	AgNPs
S30	13	60	30	AgNPs
S31	13	60	45	AgNPs
S32	13	60	60	AgNPs
S33	13	60	15	CuONPs
S34	13	60	30	CuONPs
S35	13	60	45	CuONPs
S36	13	60	60	CuONPs
S37	13	60	15	CoNPs
S38	13	60	30	CoNPs
S39	13	60	45	CoNPs
S40	13	60	60	CoNPs
S41	13	60	15	TMNPs
S42	13	60	30	TMNPs
S43	13	60	45	TMNPs
S44	13	60	60	TMNPs

Effect of pH

pH is a critical parameter that influences the reduction efficiency of silver, copper, and cobalt ions during nanoparticle synthesis. In acidic environments, there is no formation of green nanoparticles, whereas in basic conditions, the reaction is enhanced (El-Rafie et al. 2016a, b; Vanlalveni et al. 2021). Figure 1 and Table 2 (samples S1–S12) illustrate that the effect of pH was systematically investigated by maintaining a constant temperature of 60 °C and a reaction time of 60 min while varying the pH from 11 to 13. The findings revealed that as the pH increased, the absorbance of the reaction mixture also increased, with the highest absorbance and a well-defined sharp peak observed at pH 13, indicating optimal nanoparticle formation. Around 447 nm was the ideal peak for silver nanoparticles, 252 nm for CuONPs, 251 nm for CoNPs, 220 nm and 420 nm for TMNPs (El-Bisi et al. 2013).

Effect of temperature

The previous findings showed that temperature affected NPs synthesis; the higher the temperature, the faster and more uniform the nanoparticles formed. When the temperature of the synthesis was changed, there was a considerable change in both the size and the shape of the nanoparticles as illustrated in Fig. 2 and Table 2 (samples S13–S28) demonstrate that the growth behavior of the nanoparticles was altered as the temperature changed. The investigation of the absorption spectra of AgNPs, CuONPs, CoNPs, and TMNPs was performed at constant time and pH across a range of temperatures (40 °C, 50 °C, 60 °C, and 70 °C). The results indicated that as the temperature increased, the absorbance of the nanoparticles also increased gradually. Notably, most samples exhibited maximum absorbance at 60 °C. However, when the temperature exceeded 60 °C, the maximum absorbance peaks shifted to undesired wavelengths, suggesting that 60 °C is the optimal synthesis temperature. The peaks of silver nanoparticles were found

to be ideal at around 447 nm, CuONPs at 260 nm, CoNPs at 248 nm, while TMNPs contain two peaks, one at 225 nm and the other at 450 nm (Mukaratirwa-Muchanyereyi et al. 2022).

Effect of time

The effect of reaction duration was systematically evaluated by recording the absorption spectra of AgNPs, CuONPs, CoNPs, and TMNPs synthesized at a constant temperature of 60 °C and a pH of 13 across various time intervals (15 min, 30 min, 45 min, and 60 min). Figure 3 and Table 2 (samples S29–S44) illustrate that an increase in reaction time correlates with a progressive increase in absorbance, reaching its peak at 60 min. Therefore, it was determined that the optimum reaction time is 60 min. Based on these optimal conditions (60 min, pH 13, and 60 °C), the maximum peaks of silver NPs were at around 435 nm, CuONPs at 250 nm, CoNPs at 240 nm, and TMNPs have two peaks at 225 nm and at 420 nm. Samples prepared for further characterization via XRD, TEM, and SEM, as well as for additional applications, were synthesized to ensure consistent and enhanced nanoparticle formation (Veerasamy et al. 2011).

When analyzing the XRD spectrum, the crystalline nanoparticles were identified based on both the position and the relative intensity of the diffraction peaks. Table 3 and Fig. 4 shows the XRD patterns for the synthesized nanoparticles and the trimetallic nanoparticles (TMNPs). For AgNPs, the peaks at 38.7°, 44.6°, 64.50°, and 78.33° have been attributed to the (111), (200), (220), and (311) planes, respectively, as confirmed by the JCPDS file number 03-0921.

Similarly, the diffraction pattern of CuONPs revealed peaks at 32.63°, 35.24°, 38.08°, 48.45°, 53.12°, 58.34°, 61.16°, 65.96° and 67.66°. These peaks correspond to the (110), (002), (200), (202), (020), (202), (113), (022) and (220) crystallographic planes, in agreement with JCPDS card no. (89-2531))Suresh et al. 2016).

For CoNPs, the observed peaks at 31.91°, 38.10°, 39.21°, 45.0°, 58.10° and 66.16° were assigned to the (220), (311), (222), (400), (511), and (440) planes, in

Table 3 Crystallite size and lattice parameters of AgNPs, CuONPs, CoNPs, and TMNPs

	AgNPs	CuONPs	CoNPs	TMNPs
Crystallite size	11.98 nm	33.51 nm	27.47 nm	43.26 nm
Lattice parameters	a = 0.408 nm	a = 0.507 nm	a = 0.243nm	a = 4.862 nm
		b = 0.361 nm	b = 0.243 nm	
		c = 0.568 nm	c = 0.382 nm	

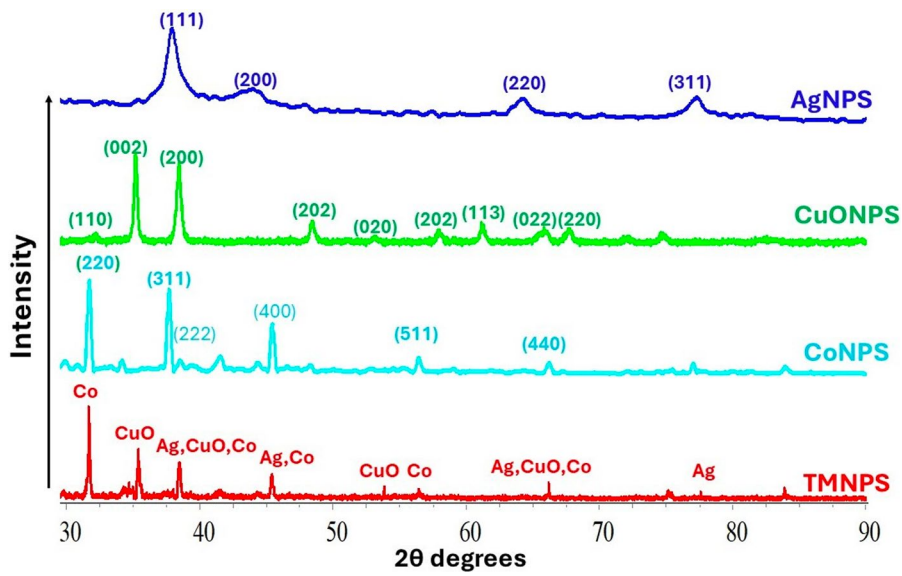


Fig. 4 XRD patterns of AgNPs, CuONPs, CoNPs, and TMNPs

agreement with JCPDS card no. 80-1538. (Prabaharan et al. 2017; Jadhav et al. 2021).

Additionally, the XRD pattern of the TMNPs shows several distinct peaks that match the Co, Ag, and CuO nanoparticles, confirming that the trimetallic nanoparticles were successfully synthesized. In the TMNPs spectra, lattice planes 110, 111, 202, 113, 311, and 004 copper oxide NPs are represented by diffraction peaks of 2 values of 32.12°, 35.33°, 38.21°, 58.15°, 67.86°, and 77.54° respectively. Lattice planes of silver NPs are represented by lattice planes 111, 200, 220, 311, and 222, which were assigned to 38.21°, 45.13°, 68.23°, 77.54°, and 83.14°. lattice planes of CoNPs, the observed peaks at 32.12°, 33.89°, 38.21°, 45.15°, 58.15°, and 67.86° were assigned to the (220), (311), (222), (400), (511), and (440) planes (Albeladi et al. 2020; Khanal et al. 2022; Abd El-Aziz and Farahat 2023).

To verify the presence of nanoparticles on the fabric surface, scanning electron microscopy (SEM) analysis was performed. As illustrated in Fig. 5, the cotton fabric samples are before and after washing.

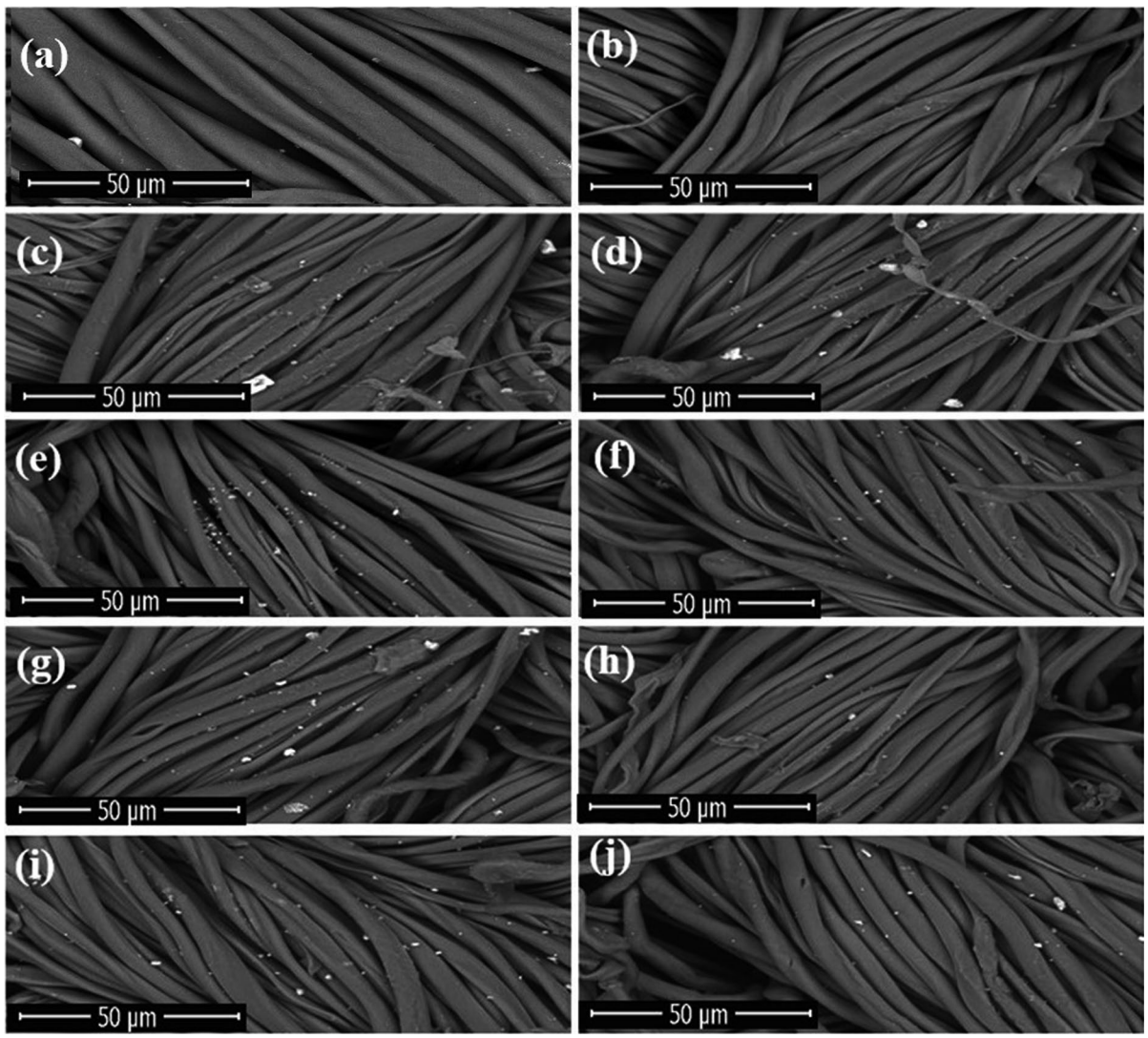


Fig. 5 SEM images of cotton fabric samples **a**, **b** fabric treated with PS, **c**, **d** fabric treated with AgNPs, **e**, **f** fabric treated with CoNPs, **g**, **h** fabric treated with CuONPs, and **i**, **j** fabric treated with TNNPs where (**a**,**c**,**e**,**g**,**i**) represent unwashed samples, (b,d,f,h, j) represent washed samples

Although some aggregated particles remain apparent on the fabric surface, nanosized silver nanoparticles (AgNPs), copper oxide nanoparticles (CuONPs), cobalt nanoparticles (CoNPs), and trimetallic nanoparticles (TMNPs) were observed on both washed and unwashed fabric samples. Notably, both the sample that had been washed and the sample that had not been washed demonstrated a specific quantity of these particles. A higher concentration of these particles was found in the sample that had not been washed, in comparison to the sample that had been washed. It was observed that TMNPs and CoNPs are well dispersed on the fabric, with a large number when compared with other samples. These findings confirm the wash fastness (Hebeish et al. 2011; Sedighi et al. 2014; Sharaf et al. 2016).

An illustration of the elemental composition of AgNPs, CuONPs, CoNPs, and TMNPs can be found in the EDX spectra (Figs S1 and S2). Figure S1 a indicates the presence of silver (Ag) with an estimated weight percentage of 5.8; Fig. S1b depicts the EDX of CuONPs, which confirms the presence of copper and oxygen with a weight percentage of 2.93 for copper and 65.2 for oxygen. The EDX of CuONPs was displayed in Fig. S1b, which confirmed the presence of copper and oxygen with a weight percentage of 2.93 for copper and 65.2 for oxygen. The percentage of copper was 5.8. The existence of cobalt is demonstrated by the weight percentage of 12.35, which is shown in Fig. S2c. Fig. S2d provides evidence that silver, copper, oxygen, and cobalt are present, with the respective weight percentages of 1.23, 3.05, 63.49, and 1.86 representing the presence of these elements. The residual PS was responsible for the presence of signals for oxygen (O), carbon (C), and nitrogen (N) atoms in the NPs, which were found in all the spectra shown in Figs. S1 and S2 (Huq et al. 2020; Chelliah et al. 2023; Naikoo et al. 2023; Kolahalam et al. 2024).

Transmission electron microscopy (TEM) was utilized to determine the morphology, particle size, and distribution of the biosynthesized nanoparticles

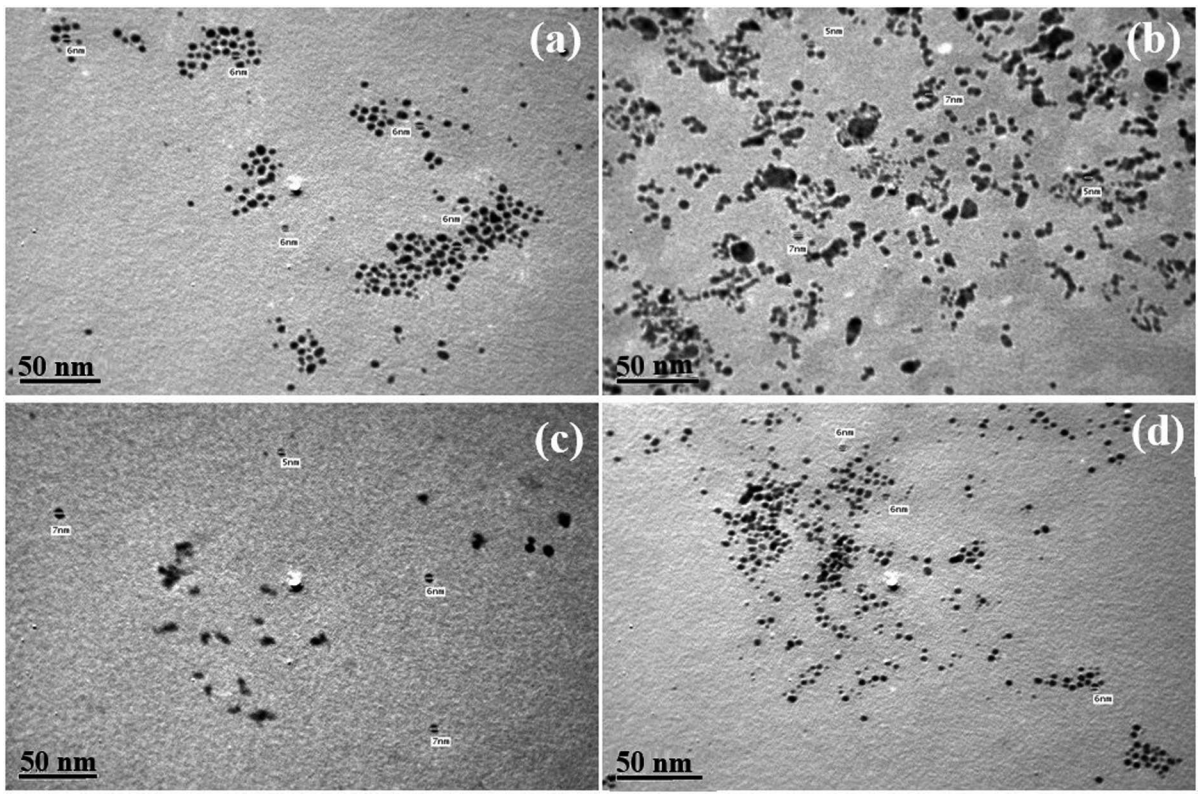


Fig. 6 TEM images of **a** AgNPs, **b** CuONPs, **c** CoNPs, and **d** TMNPs

(NPs). For sample preparation, 1 mL of the reaction mixture containing AgNPs, CuONPs, CoNPs, and TMNPs was subjected to water bath sonication. Subsequently, a drop of the mixture was deposited onto a copper grid coated with a carbon film (200 mesh) and allowed to dry under vacuum conditions. As illustrated in Fig. 6 the TEM images of the monometallic nanoparticles confirm that AgNPs, CuONPs, CoNPs, and TMNPs. For AgNPs, the particle sizes were at about 6nm; the particles are spherical and well dispersed. For CuONPs, the particle sizes range from 5 to 10 nm, and the particles are not well dispersed and show some aggregation. For CoNPs, the particle sizes range from 5 to 8 nm, the particles are well dispersed, and they are spherical in shape. For TMNPs with particle sizes ranging from 6 to 9 nm, the particles are spherical in shape, well dispersed, and have well-identified morphology. We found that AgNPs and TMNPs exhibited uniform distribution and superior morphological characteristics, while CuONPs and CoNPs showed some degree of aggregation (Abhinav et al. 2015; Hafeez et al. 2020; Chandrasekharan et al. 2022; Giri et al. 2022).

Fourier transform infrared (FT-IR) spectroscopy was employed to identify the functional groups involved in the reduction of metal ions to nanoparticles (NPs), thereby contributing to the stability of the synthesized NPs. In all examined spectra (Fig. 7A–E), several characteristic absorption bands were observed. Specifically, the broad band in the range of 3650–3250 cm^{-1} corresponds to the –O–H stretching vibration. The bands observed from 3000 to 2850 cm^{-1} are attributed to sp^3 C–H stretching vibrations. Additionally, the absorption band noted between 1700 and 1800 cm^{-1} is associated with the carbonyl functional group. The IR spectra further reveal a band between 1600 and 1630 cm^{-1} that is indicative of the alkenyl aliphatic (C=C stretching) vibration, along with another band from 1400 to 1600 cm^{-1} corresponding to the alkenyl aromatic (C=C stretch) vibration. Moreover, a bending vibration of C–H bonds is evident in the range of 1350–1400 cm^{-1}, while a vibration observed between 1078.26 and 1300 cm^{-1} is attributable to the C–O stretching vibration, the functional groups O–H, C=O, C=C are responsible for reduction of ions to NPs. These results underscore the role of specific functional groups in stabilizing the nanoparticles during synthesis, which is critical for their subsequent application in various fields of research (Masri et al. 2018; Das et al. 2020; Aslam et al. 2021; Okaiyeto et al. 2021).

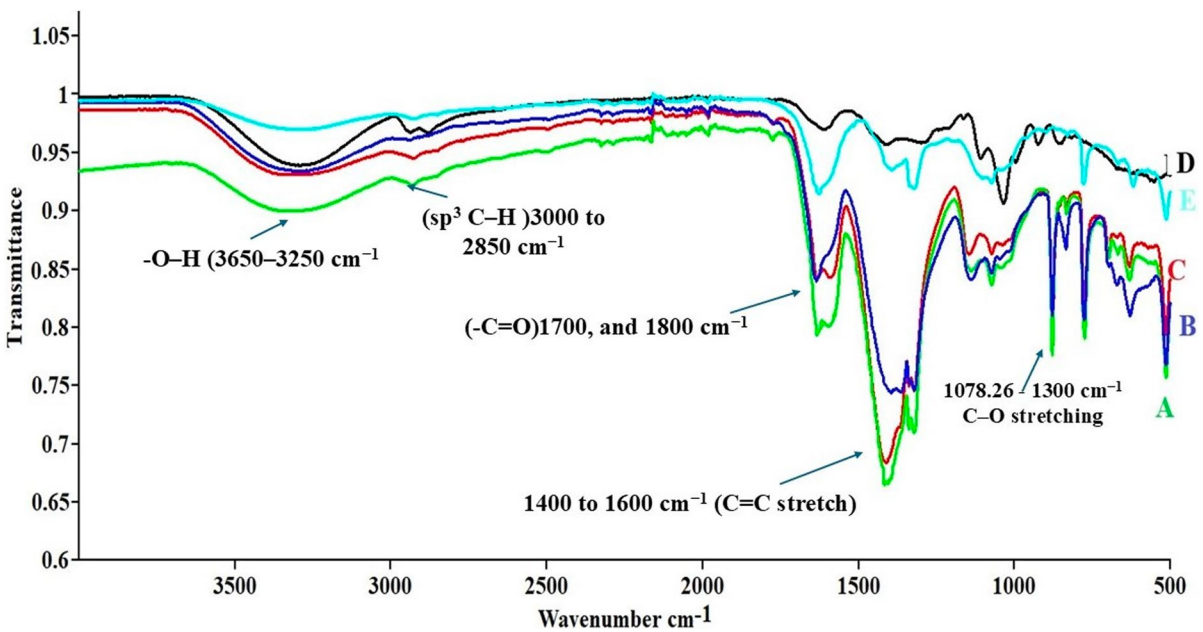


Fig. 7 FT-IR spectra of **A** PS, **B** AgNPs **C** CuONPs, **D** CoNPs, **E** TMNPs

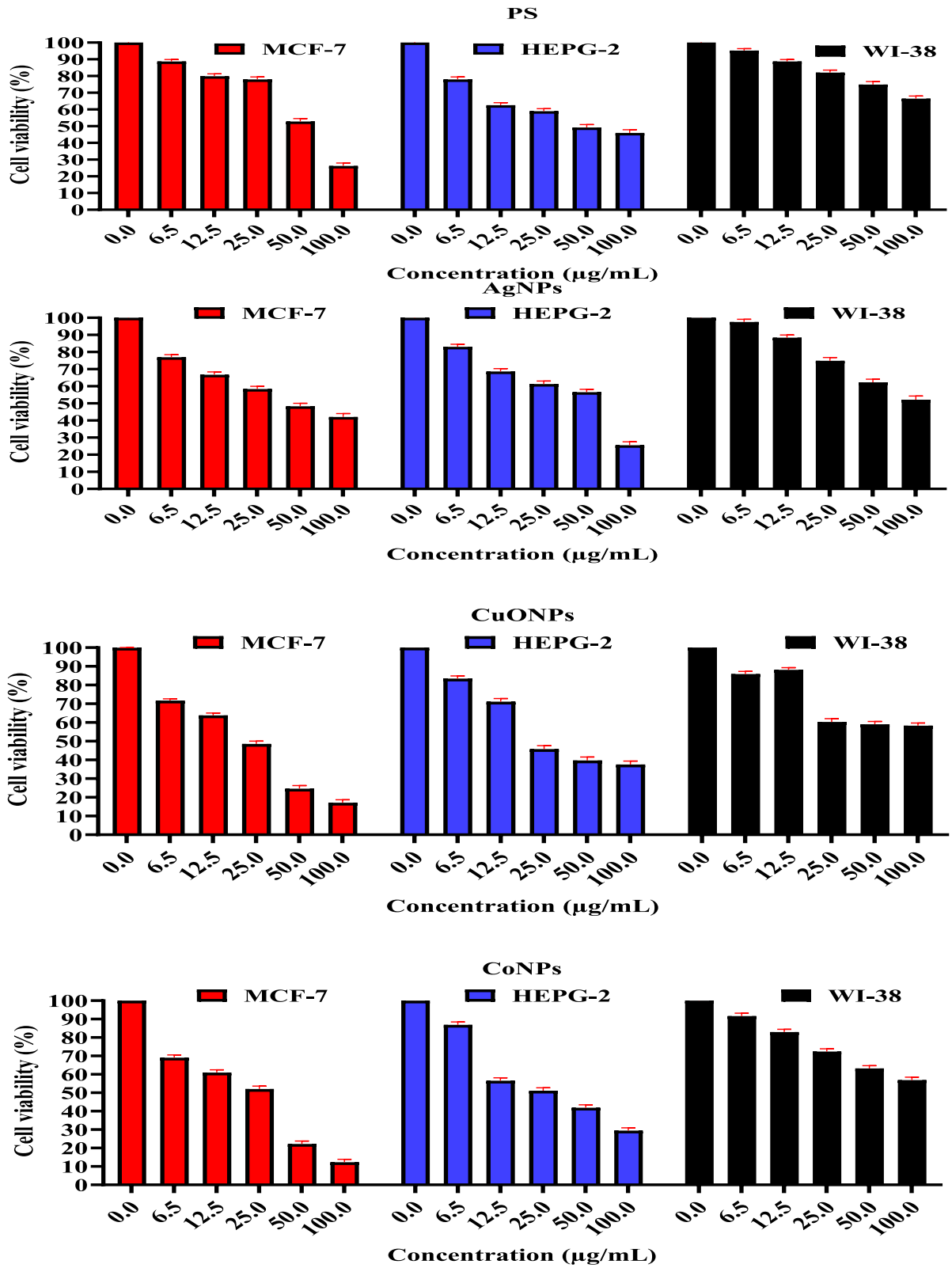


Fig. 8 Cytotoxicity results of PS, AgNPs, CuONPs, CoNPs, and TMNPs

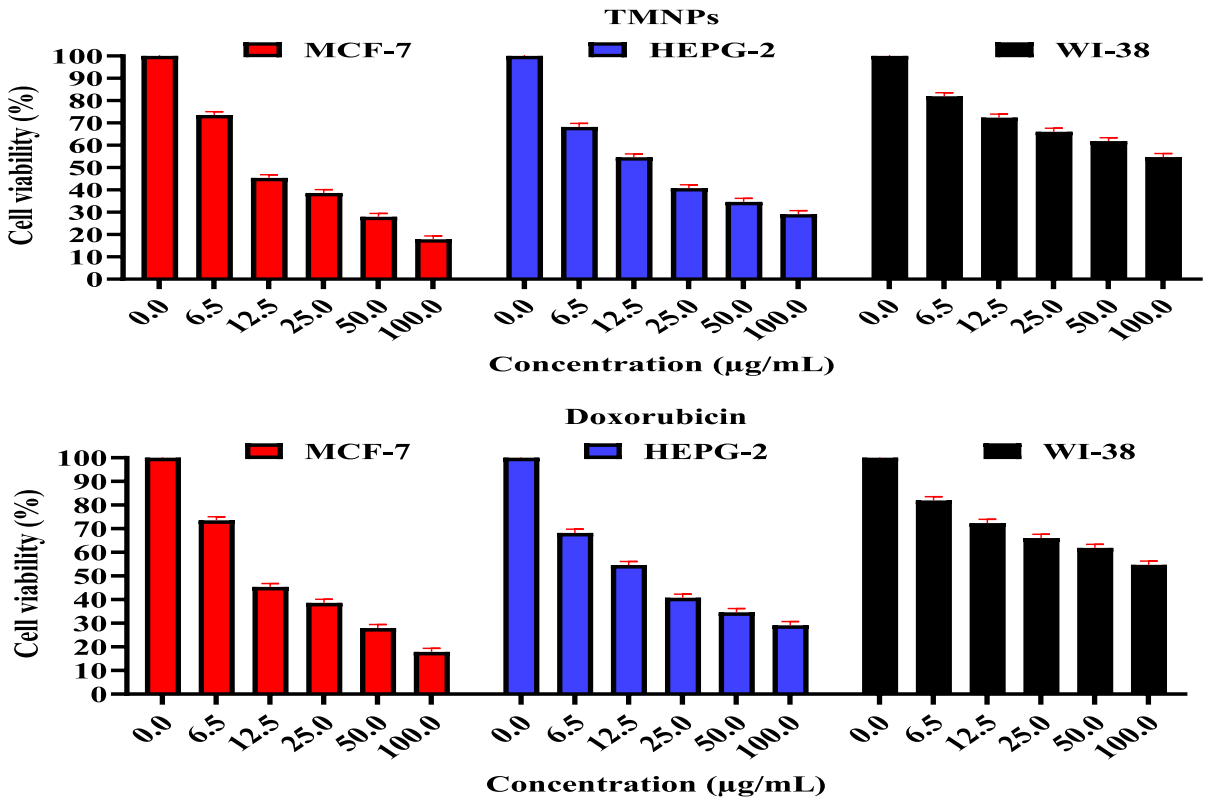


Fig. 8 (continued)

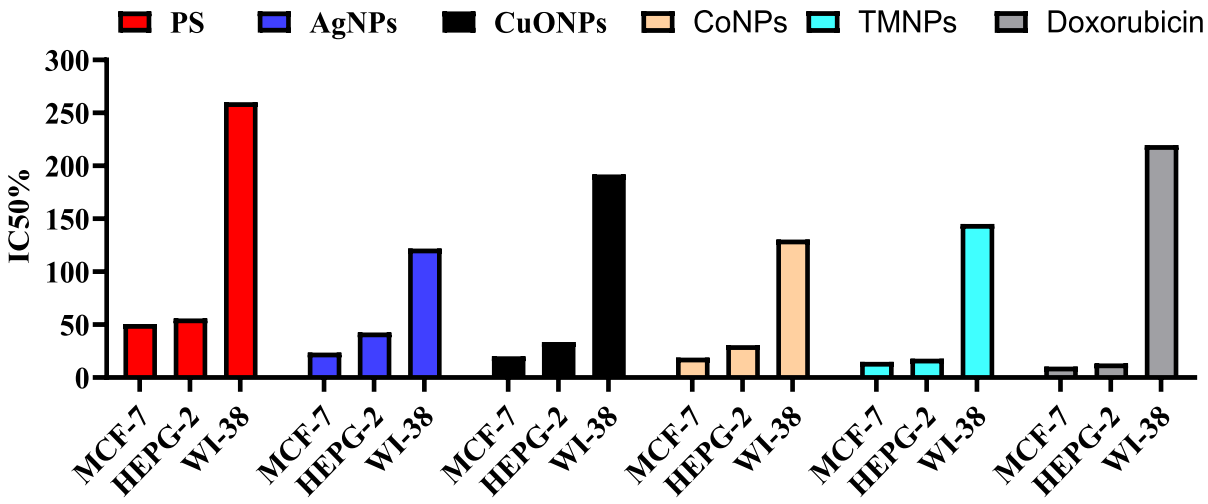


Fig. 9 Bar graph illustrates the IC_{50} of MCF-7, HEPG-, and WI-38

Table 4 Anti-inflammatory activity of AgNPs, CuONPs, CoNPs, TMNPs, and S.S Ointment

Treatment	Zero (mm)	1 h paw diameter (mm)	1 h oedema (mm)	1 h % inhibition	1 h *p*-value	2 h paw diameter (mm)	2 h oedema (mm)	2 h % inhibition	2 h *p*-value	3 h paw diameter (mm)	3 h oedema (mm)	3 h % inhibition	3 h *p*-value	4 h paw diameter (mm)	4 h oedema (mm)	4 h % inhibition	4 h *p*-value
Control	3.35 ± 0.29	4.52 ± 0.39*	1.17	–	–	4.81 ± 0.38*	1.46	–	–	4.92 ± 0.31*	1.57	–	–	4.97 ± 0.42*	1.62	–	–
PS	3.25 ± 0.19	4.13 ± 0.42*	0.88	24.78 ± 0.9	0.03*	4.05 ± 0.1*	0.80	45.20 ± 0.7	0.01**	4.00 ± 0.11*	0.75	52.22 ± 1.51	0.02*	3.95 ± 0.11*	0.70	56.79 ± 1.60	0.04*
PS 10w	3.28 ± 0.29	4.20 ± 0.42*	0.92	21.36 ± 0.8	0.06	4.10 ± 0.11*	0.82	43.38 ± 0.81	0.03*	4.05 ± 0.1*	0.77	50.90 ± 1.43	0.05	4.01 ± 0.11*	0.73	54.90 ± 1.51	0.07
AgNPs	3.28 ± 0.34	4.09 ± 0.42*	0.81	30.76 ± 1.3	0.02*	4.15 ± 0.1*	0.71	51.37 ± 0.89	0.01**	3.97 ± 0.36*	0.63	59.87 ± 1.71	0.005**	3.99 ± 0.07*	0.55	66.05 ± 1.79	0.01**
AgNPs 10w	3.10 ± 0.14	4.27 ± 0.1*	0.83	29.06 ± 1.1	0.04*	4.05 ± 0.36*	0.74	49.32 ± 0.91	0.02*	4.06 ± 0.1*	0.64	59.24 ± 1.52	0.03*	3.91 ± 0.36*	0.60	62.96 ± 1.43	0.05
CuONPs	3.53 ± 0.04	4.08 ± 0.1*	0.55	52.59 ± 1.4	0.001**	4.11 ± 0.01*	0.48	67.12 ± 1.11	0.0005**	3.94 ± 0.05*	0.41	73.89 ± 2.01	0.0001**	3.85 ± 0.01*	0.32	80.25 ± 2.45	0.0001**
CuONPs 10w	3.27 ± 0.29	3.91 ± 0.37*	0.64	45.30 ± 1.5	0.01**	3.79 ± 0.34*	0.52	64.38 ± 1.09	0.002**	3.70 ± 0.28*	0.43	72.61 ± 1.91	0.001**	3.64 ± 0.22*	0.37	77.16 ± 1.93	0.001**
CoNPs	3.50 ± 0.08	4.11 ± 0.1*	0.61	47.41 ± 1.7	0.003**	4.05 ± 0.01*	0.55	62.33 ± 1.61	0.001**	3.99 ± 0.06*	0.49	68.79 ± 1.61	0.0005**	3.92 ± 0.03*	0.42	74.07 ± 1.59	0.0002**
CoNPs 10w	3.34 ± 0.31	4.03 ± 0.31*	0.69	41.03 ± 1.41	0.02*	3.97 ± 0.41*	0.63	56.85 ± 1.52	0.01**	3.85 ± 0.29*	0.51	67.52 ± 1.84	0.02*	3.79 ± 0.21*	0.45	72.22 ± 1.89	0.03*
TMNPs	3.45 ± 0.02	3.49 ± 0.04*	0.49	58.12 ± 1.49	0.0001**	3.72 ± 0.33*	0.41	71.92 ± 1.72	0.0001**	3.59 ± 0.39*	0.28	82.17 ± 2.31	0.0001**	3.52 ± 0.35*	0.21	87.04 ± 2.11	0.0001**
TMNPs 10w	3.31 ± 0.26	3.84 ± 0.38*	0.53	54.70 ± 1.37	0.001**	3.87 ± 0.06*	0.42	71.23 ± 1.81	0.0005**	3.80 ± 0.07*	0.35	77.71 ± 1.98	0.0001**	3.74 ± 0.19*	0.29	82.10 ± 1.93	0.0001**
S.S Oint	3.33 ± 0.19	3.79 ± 0.35*	0.46	60.68 ± 1.5	0.0001**	3.69 ± 0.26	0.36	75.34 ± 1.88	0.0001**	3.59 ± 0.12*	0.26	83.44 ± 1.69	0.0001**	3.51 ± 0.17*	0.18	88.89 ± 1.73	0.0001**

The anticancer activity

Two cancer cell lines were utilized to evaluate the dose-dependent inhibitory effects of polysaccharides (PS) and nanoparticles (NPs) on cancer cells, thereby assessing their anticancer potential. Owing to the known deleterious side effects associated with many conventional drugs, a green-synthesized chemotherapeutic agent incorporating silver (AgNPs), copper oxide (CuONPs), cobalt (CoNPs), and trimetallic nanoparticles (TMNPs) was developed (Alkhathlan et al. 2021).

The cytotoxicity and safety of PS, AgNPs, CuONPs, CoNPs, and TMNPs were investigated using MCF-7, HEPG-2, and WI-38 cell lines, as detailed in Table S1 and Figs. 8 and 9. Following a 24 h incubation period, the agents were administered at concentrations of 0 µg/mL, 6.5 µg/mL, 12.5 µg/mL, 25 µg/mL, 50 µg/mL, and 100 µg/mL. The percentage of cell viability was calculated based on the optical density (OD) values obtained from the MTT assay.

At the lowest concentration, all formulations (PS, AgNPs, CuONPs, CoNPs, and TMNPs) exhibited minimal cytotoxicity, whereas an increase in NP concentration resulted in a corresponding decrease in cell viability. This dose-dependent reduction indicates potent anticancer activity of the synthesized nanoparticles. Specifically, TMNPs demonstrated the highest cytotoxicity in MCF-7 cells, with an IC_{50} value of 14.7 µg/mL, which is an improvement over the previously reported value of 19.44 µg/mL. Similarly, CuONPs and AgNPs exhibited IC_{50} values of 20.0 µg/mL and 23.5 µg/mL, respectively, compared to earlier reported values of 45.95 µg/mL for CuONPs and 56.83 µg/mL for AgNPs (Abd El-Aziz and Farahat 2023). In contrast, CoNPs and PS recorded IC_{50} values of 18.79 µg/mL and 50.6 µg/mL, respectively.

In normal lung cells (WI-38), CuONPs and AgNPs demonstrated IC_{50} values of 191.9 µg/mL and 121.9 µg/mL, respectively indicating enhanced cell viability compared to previous studies that reported an IC_{50} of 115.9 µg/mL. TMNPs and CoNPs in WI-38 cells showed IC_{50} values of 145 µg/mL and 130.3 µg/mL, respectively. For HEPG-2 cells, TMNPs again exhibited the greatest cytotoxicity with an IC_{50} of 17.81 µg/mL, followed by CoNPs at 30.53 µg/mL, CuONPs at 33.7 µg/mL, AgNPs at 42.6 µg/mL, and PS at 55.98 µg/mL (Bhavi et al. 2024a, b, c; Bhavi et al. 2025).

The results indicate that PS is the safest among the tested agents, as it maintains a high cell viability in normal lung cells, while the nanoparticles demonstrate strong anticancer effects. The results also reveal a synergistic effect when these nanoparticles are combined, as the therapeutic activity of TMNPs exceeds that of any monometallic nanoparticles alone. TMNPs' have superior cytotoxicity as they are capable of operating through multiple mechanisms. This synergistic benefit underlines the potential for combination therapy, wherein the integrated therapeutic effect is greater than the sum of the individual effects (Siddiqui et al. 2013; Koyyati et al. 2016;

Table 5 Effect of PS, AgNPs, CuONPs, CoNPs and TMNPs on wound healing area

Group	Zero time (cm^2)	Day 4 (cm^2)	Day 10 (cm^2)	% Inhibition (day 4)	% Inhibition (day 10)
Control	1.58 ± 0.23	1.51 ± 0.11*	1.42 ± 0.24*	4.43 ± 0.24*	10.13 ± 0.31*
PS	1.43 ± 0.12	1.20 ± 0.19*	0.85 ± 0.21*	16.08 ± 0.51*	40.55 ± 0.71*
PS 10W	1.44 ± 0.14	1.25 ± 0.19*	0.89 ± 0.21*	13.19 ± 0.41*	38.19 ± 0.61*
AgNPs	1.46 ± 0.13	1.12 ± 0.29*	0.79 ± 0.21*	23.29 ± 0.52*	45.89 ± 0.79*
AgNPs 10W	1.45 ± 0.02	1.20 ± 0.02*	0.80 ± 0.25*	17.24 ± 0.44*	44.82 ± 0.81*
TMNPS	1.41 ± 0.11	0.61 ± 0.28*	0.21 ± 0.06*	56.74 ± 0.61*	85.11 ± 1.11*
TMNPS 10W	1.43 ± 0.11	0.71 ± 0.29*	0.29 ± 0.10*	50.34 ± 0.71*	79.72 ± 1.01*
CuONPs	1.39 ± 0.16	0.89 ± 0.33*	0.52 ± 0.21*	35.97 ± 0.55*	62.59 ± 1.22*
CuONPs 10W	1.38 ± 0.19	0.99 ± 0.35*	0.59 ± 0.23*	28.26 ± 0.45*	57.24 ± 0.87*
CoNPs	1.33 ± 0.18	0.91 ± 0.34*	0.68 ± 0.36*	31.58 ± 0.61*	48.87 ± 0.71*
CoNPs 10W	1.34 ± 0.19	0.98 ± 0.38*	0.78 ± 0.38*	26.86 ± 0.57*	41.79 ± 0.87*
S.S Oint	1.59 ± 0.17	0.51 ± 0.25*	0.04 ± 0.001*	67.93 ± 0.98*	97.94 ± 1.66*

* Statistically significantly different from zero time at $P < 0.05$

Ramaswamy et al. 2016; Khorrami et al. 2018; Ganesan et al. 2020; Rajeshkumar et al. 2024; Abd El-Aziz et al. 2024).

Anti-inflammatory activity

The anti-inflammatory properties of cloth treated with polysaccharides (PS) and nanoparticles (NPs), as well as the impact of subjecting the material to ten washing cycles, were rigorously evaluated. The assessments were based on the determination of the percentage of Oedema and the percentage of oedema inhibition, which were calculated using the following formulas:

$$\%\ \text{Oedema} = \frac{\text{wt. of right paw} - \text{wt. of left paw}}{\text{wt. of left paw}} \times 100 \quad (2)$$

$$\%\ \text{Oedema Inhibition} = \frac{Mc - Mt}{Mc} \times 100 \quad (3)$$

Here, *Mc* represents the percentage Oedema observed in the control group, while *Mt* corresponds to the percentage Oedema observed in the NPs-treated group. This methodological approach provides a quantitative framework for comparing the efficacy of different treatments, as well as the durability of their anti-inflammatory properties following multiple washes.

According to data reported in Table 4, fabrics treated with TMNPs and CuONPs exhibited notably higher anti-inflammatory activity than those treated with PS, AgNPs, and CoNPs. Specifically, the unwashed fabric treated with TMNPs demonstrated the highest level of Oedema inhibition at 87.04%, representing an improvement over the previously reported value of 84.6%. In addition, fabric treated with CuONPs showed an inhibition of 80.25% compared to the earlier reported value of 79.28%. The levels of inhibition for fabrics treated with CoNPs, AgNPs, and PS were 74.07%, 66.05%, and 56.79%, respectively. Furthermore, unwashed fabrics consistently exhibited higher Oedema inhibition relative to washed fabrics. It was also established that the washing process eliminated only a minimal percentage of the nanoparticles, a finding that is consistent with SEM analyses (Abou Zeid and Mohammed 2009; Faisal et al. 2022). The results of the anti-inflammatory activity assessment, as shown in Table 4, indicate that all tested treatments, including AgNPs, CuONPs, CoNPs, TMNPs, and S.S Ointment, have demonstrated significant anti-inflammatory effects compared to the control group at various time points post-treatment. The ANOVA analysis confirmed significant differences in paw diameter and oedema thickness among the groups ($p < 0.001$). Post-hoc t-tests revealed that treatments such as PS, PS 10w, AgNPs, AgNPs

Table 6 One-way ANOVA results

Parameter	F-value	*p*-value	Conclusion
Day 10 wound area	48.72	< 0.001*	Significant
% Inhibition (day 10)	52.89	< 0.001*	Significant

Comparison: All groups vs. Control for *Day 10 wound area* and *% Inhibition (Day 10)*.

Post-hoc tukey test: All treatment groups (PS, AgNPs, TMNPS, etc.) showed statistically significant ($p < 0.05$) improvements over Control.

Table 7 Pairwise t-tests (vs. Control)

Group	Mean diff (day 10)	t-value	*p*-value	Effect size (Cohen's d)
PS	− 0.57 cm^2	4.21	< 0.001*	1.45
AgNPs	− 0.63 cm^2	4.89	< 0.001*	1.82
TMNPS	− 1.21 cm^2	9.12	< 0.001*	3.54
CuONPs	− 0.90 cm^2	6.34	< 0.001*	2.41
CoNPs	− 0.74 cm^2	5.01	< 0.001*	1.92
S.S Oint	− 1.38 cm^2	12.45	< 0.001*	4.87

Comparison: Each treatment vs. Control for *Day 10 Wound Area*

Key: TMNPS and S.S Oint showed the largest effects ($d > 3$)

Table 8 Weathered vs. Non-Weathered Comparisons

Comparison	Mean diff (% Inhibition)	t-value	*p*-value
PS vs. PS 10W	+ 2.36%	2.87	0.012*
AgNPs vs. AgNPs 10W	+ 1.07%	1.98	0.049*
TMNPS vs. TMNPS 10W	+ 5.39%	4.76	< 0.001*
CuONPs vs. CuONPs 10W	+ 5.35%	3.92	0.002*
CoNPs vs. CoNPs 10W	+ 7.08%	5.24	< 0.001*

Paired t-tests for *day 10% inhibition* (e.g., PS vs. PS 10W)

Conclusion: Weathered (10W) groups had significantly ($p < 0.05$) reduced efficacy compared to non-weathered counterparts

Table 9 Top performers (day 10)

Group	Wound area (cm^2)	% Inhibition	vs. control (*p*-value)	vs. S.S Oint (*p*-value)
TMNPS	0.21 ± 0.06*	85.11 ± 1.11	< 0.001*	0.003*
S.S Oint	0.04 ± 0.001	97.94 ± 1.66	< 0.001*	—
CuONPs	0.52 ± 0.31	62.59 ± 1.22	< 0.001*	< 0.001*

Key: TMNPS was the best-performing nanoparticle (85.11% inhibition)

S.S Oint (positive control) was superior to all NPs ($p < 0.01$)

Weathered groups consistently underperformed non-weathered ($p < 0.05$)

10w, CuONPs, CuONPs 10w, CoNPs, CoNPs 10w, TMNPs, TMNPs 10w, and S.S Ointment all exhibited statistically significant reductions in paw diameter and oedema thickness at multiple time points (1–4h) with *p*-values ranging from 0.01 to 0.0001. Notably, the highest percentage inhibitions were observed with TMNPs, TMNPs 10w, and S.S Ointment, particularly at the 4 h mark, suggesting these treatments were the most effective at reducing inflammation. The findings suggest that nanoparticles and the S.S. Ointment have potential as therapeutic agents for inflammatory conditions, with some nanoparticle formulations showing comparable or superior efficacy to the standard S.S. Ointment. These results highlight the importance of further investigation into the mechanisms of action and potential clinical applications of these nanoformulations.

Wound healing activity

In the context of tissue repair, nanoparticles contribute to the proliferation of cells, the management of inflammation, and the decrease of scars, among other potentially beneficial therapeutic effects. They are increasingly being utilized in physiotherapy applications, where they are employed to enhance tissue regeneration and inflammation management (Cardoza et al. 2024). The rate at which the unhealed area decreases during treatment, referred to as wound contraction, serves as an indicator of therapeutic efficacy. A more substantial reduction in wound size reflects greater medication effectiveness. Scanning electron microscopy (SEM) analysis revealed that during the washing process, some polysaccharides (PS), silver nanoparticles (AgNPs), copper oxide nanoparticles (CuONPs), cobalt nanoparticles (CoNPs), and trimetallic nanoparticles (TMNPs) were released from the fabric. However, no significant difference was observed in the percentage of wound contraction between washed and unwashed cotton fabrics.

Table 5 through Table 8 collectively demonstrate that all treatments significantly enhanced wound healing compared to the control, with the most notable improvements observed in the TMNPs group. In Table 5, the data reveal that TMNPs achieved an 85.11% inhibition in wound area by Day 10 with a remaining wound area of only 0.21 ± 0.06 cm^2, outperforming other treatments such as PS, AgNPs, CuONPs, and CoNPs, while the S.S Oint, used as a positive control, produced an even greater inhibition (97.94 ± 1.66%) with the smallest wound area (0.04 ± 0.001cm^2). Table 5 confirms the overall significance of these improvements using one-way ANOVA, which provided F-values of 48.72 and 52.89 for Day 10 wound area and % inhibition, respectively, both at a *p*-value of < 0.001. Table 6's pairwise t-tests further elucidate these differences, indicating statistically significant mean differences (e.g., TMNPs exhibited a − 1.21 cm^2 reduction from control with a t-value of 9.12 and Cohen's d of 3.54) that highlight the robust therapeutic potential of these nanoparticle formulations. However, Table 7 shows that weathered formulations (10W) consistently underperformed, with significantly lower % inhibition compared to their non-weathered counterparts ($p < 0.05$), suggesting that environmental exposure can compromise efficacy. Finally, Table 8 underscores that while TMNPs demonstrated the strongest nanoparticle performance among the treatments, the S.S Oint remained superior ($p < 0.01$), providing

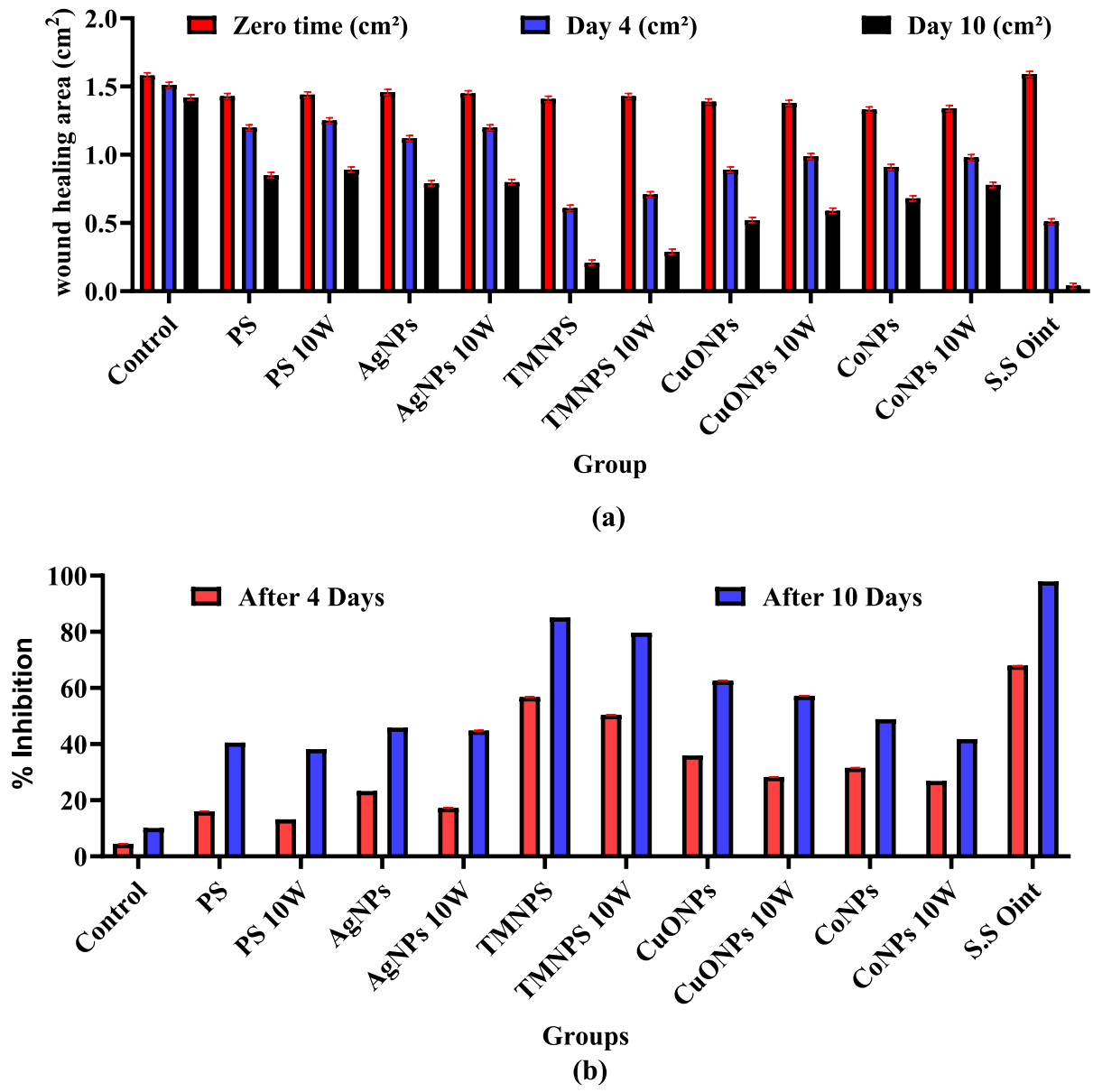


Fig. 10 Comparison of wound healing area and inhibition rate across different treatment groups **a** the wound healing area over time and **b** the percentage inhibition of wound area

a benchmark for efficacy. Table 9 showed that these integrated findings were strongly support the potential of TMNPs for biomedical applications in wound healing, albeit with the noted limitation of reduced performance under weathered conditions (Kalaiselva and Rajasekaran 2009; Krishnan et al. 2020; Sharaf et al. 2022; Bhavi et al. 2024a, b, c; Kenawy et al. 2024; Rostamitabar et al. 2022).

Figure 10a, b illustrate the wound healing performance of various treatments over 10 days. In Fig. 10a, the wound healing area (cm^2) at zero-time, day 4, and day 10 is compared across control, PS, and nanoparticle-based groups, including TMNPS 10W and S.S Oint. The results indicate that TMNPS 10W demonstrates superior wound contraction, with the smallest residual area at day 10 compared

to other groups, including the standard S.S Oint. Notably, the control group exhibits minimal healing, emphasizing the efficacy of the tested treatments. In Fig. 10b, the percentage inhibition of wound area after 4 and 10 days further highlights TMNPS 10W's effectiveness, achieving over 90% inhibiting by day 10. This outperforms other groups, such as PS, AgNPs, and CuONPs, which show lower inhibition rates, particularly on day 4. The enhanced performance of TMNPS 10W is attributed to its optimized nanomaterial properties, which likely promote faster tissue repair and antimicrobial activity. While S.S. Oint shows moderate efficacy, its inhibition rate remains lower than TMNPS 10W, underscoring the potential of engineered nanomaterials in wound management. These findings suggest that TMNPS 10W could be a promising therapeutic candidate for accelerating wound healing.

Conclusion

The study demonstrates that the use of polysaccharides extracted from *M. crystallinum* enables a rapid, scalable, and environmentally friendly synthesis of nanoparticles. The produced cobalt (CoNPs), copper oxide (CuONPs), silver (AgNPs), and trimetallic nanoparticles (TMNPs) are monodispersed, spherical, and range from 2 to 15 nm, confirming that this green approach reliably produces particles with consistent morphological features. Importantly, the biologically derived nanoparticles display significant anticancer**,** anti-inflammatory, and wound-healing properties, which underscore their potential in medical applications. Future efforts should concentrate on optimizing particle properties, which entail fine-tuning synthesis parameters to further control particle size and distribution. Additionally, it is crucial to gain mechanistic insights (Narayana et al. 2024) by investigating the underlying biochemical interactions that drive the observed bioactivity. Such knowledge will help in refining the synthesis protocols and enhancing the functional properties of nanoparticles. Moreover, to fully harness their therapeutic potential, emphasis must be placed on the clinical translation of these materials. This involves transitioning from in vitro assessments to in vivo studies to validate both therapeutic efficacy and safety, ultimately paving the way toward effective clinical applications.

Author Contributions A-Hussein H Hammam: methodology, data analysis; B-E.M. KHALIL: supervision; C- Ahmed H. I. Faraag contributed to the analysis of the data; D-Salim Mohamed Abd El-Aziz: The conceptualization, research design, methodology, data analysis, data curation, writing of the initial draft, reviewing, editing, and supervision of the whole work.

Funding Open access funding provided by The Science, Technology & Innovation Funding Authority (STDF) in cooperation with The Egyptian Knowledge Bank (EKB). Not applicable.

Data availability No datasets were generated or analysed during the current study.

Declarations

Conflict of interest The authors declare no conflict of interest.

Ethical approval The current experimental design was approved by the research ethical committee of Science Faculty, Helwan University (approval no. REC-Sci- HU/C92-08–02).

Consent for publication Not applicable.

Open Access This article is licensed under a Creative Commons Attribution 4.0 International License, which permits use, sharing, adaptation, distribution and reproduction in any medium or format, as long as you give appropriate credit to the original author(s) and the source, provide a link to the Creative Commons licence, and indicate if changes were made. The images or other third party material in this article are included in the article's Creative Commons licence, unless indicated otherwise in a credit line to the material. If material is not included in the article's Creative Commons licence and your intended use is not permitted by statutory regulation or exceeds the permitted use, you will need to obtain permission directly from the copyright holder. To view a copy of this licence, visit http://creativecommons.org/licenses/by/4.0/.

References

Aachary A, Prapulla G (2011) Xylooligosaccharides (XOS) as an emerging prebiotic: microbial synthesis, utilization, structural characterization, bioactive properties, and applications. Compr Rev Food Sci Food Saf 10(1):2–16. https://doi.org/10.1111/j.1541-4337.2010.00135.x

Abbigeri MB, Thokchom B, Bhavi SM, Singh SR, Joshi P, Yarajarla RB (2024) Potential in vitro antibacterial and anticancer properties of biosynthesized multifunctional silver nanoparticles using Martynia annua L. leaf extract. Nano-Struct Nano-Objects 39:101320. https://doi.org/10.1016/j.nanoso.2024.101320

Abd El-Aziz M, Farahat A (2023) The activity of *Vossia cuspidata* polysaccharides-derived monometallic CuO, Ag, Au, and trimetallic CuO-Ag-Au nanoparticles against cancer, inflammation, and wound healing. J Inorg Organomet Polym 33:853–865. https://doi.org/10.1007/s10904-023-02542-x

Abd El-Aziz SM, Faraag AH, Abdul-Baki EA, Fouda MS (2024) Enhancement of *Cinnamomum camphora* magnetic nanoparticle bioactivities via carboxymethyl cellulose immobilization for potential therapeutic applications in cancer treatment. Cellulose. https://doi.org/10.1007/s10570-024-06104-3

Abhinav V, Rao K, Karthik S, Singh P (2015) Copper conductive inks: synthesis and utilization in flexible electronics. RSC Adv 5(79):63985–64030. https://doi.org/10.1039/C5RA08205F

Abou Hussein M, Abdel Maksoud A, Fahim A, Awed S (2021) Unveiling the gamma irradiation effects on linear and nonlinear optical properties of CeO_2–Na_2O–SrO–B_2O_3 glass. Opt Mater 114:111007. https://doi.org/10.1016/j.optmat.2021.111007

Abou Zeid H, Mohammed S (2009) Phenolic compounds and biological activities of Dichrostachys cinerea L. Med Aromatic Plant Sci Biotechnol 3:42–49

Alaa R, Abd-Alhaseeb M, Habib S, Ibrahim K, Ahmed A (2016) Screening of *Marrubium alysson* L. extract for pharmacological activity. J Chem Pharm Res 8(4):283–289

Albeladi R, Malik A, Al-thabaiti A (2020) Facile biofabrication of silver nanoparticles using *Salvia officinalis* leaf extract and its catalytic activity towards Congo red dye degradation. JMR T 9(5):10031–10044. https://doi.org/10.1016/j.jmrt.2020.06.074

Al-darwesh MY, Babakr KA, Qader IN (2024a) Characterization and anticancer evaluation of zirconia nanoparticles synthesized via green route using *Sophora flavescens* roots extract. Nano-Struct Nano-Objects 39:101245. https://doi.org/10.1016/j.nanoso.2024.101245

Al-darwesh MY, Ibrahim SS, Hamid LL (2024b) *Ficus carica* latex mediated biosynthesis of zinc oxide nanoparticles and assessment of their antibacterial activity and biological safety. Nano-Struct Nano-Objects 38:101163. https://doi.org/10.1016/j.matchemphys.2025.130517

Al-darwesh MY, Ibrahim SS, Mohammed MA (2024c) A review on plant extract mediated green synthesis of zinc oxide nanoparticles and their biomedical applications. Results Chem 7:101368. https://doi.org/10.1016/j.rechem.2024.101368

Al-darwesh MY, Babakr KA, Qader IN, Mohammed MA (2025a) Antimicrobial, anti-inflammatory, and anticancer potential of green synthesis TiO2 nanoparticles using *Sophora flavescens* root extract. Chem Pap 79(2):1207–1221. https://doi.org/10.1007/s11696-024-03853-0

Al-darwesh MY, Hamid LL, Ibrahim SS, Mohammed MA (2025b) Construction and characterization of 5, 6-O-isopropylidene-L-ascorbic acid-loaded silver and manganese dioxide nanoparticles: cytotoxicity study, antibacterial, and antioxidant activities. Mater Chem Phys. https://doi.org/10.1016/j.matchemphys.2025.130517

Al-Haddad J, Alzaabi F, Pal P, Rambabu K, Banat F (2020) Green synthesis of bimetallic copper–silver nanoparticles and their application in catalytic and antibacterial activities. Clean Technol Environ Policy 22(1):269–277. https://doi.org/10.1007/s10098-019-01765-2

Alkhathlan H, Al-Abdulkarim A, Khan M, Khan M, Alkholief M, Alshamsan A, Almomen A, Albekairi N, Alkhathlan Z, Siddiqui H (2021) Evaluation of the anticancer activity of phytomolecules conjugated gold nanoparticles synthesized by aqueous extracts of Zingiber officinale (Ginger) and Nigella sativa L. Seeds (Black Cumin). Materials 14(12):3368. https://doi.org/10.3390/ma14123368

Allemailem KS, Khadri H, Azam M, Khan MA, Rahmani AH, Alrumaihi F, Almatroudi A (2022) Ajwa-dates (*Phoenix dactylifera*)-mediated synthesis of silver nanoparticles and their anti-bacterial, anti-biofilm, and cytotoxic potential. Appl Sci 12(9):4537. https://doi.org/10.3390/app12094537

Al-Marhaby F, Seoudi R (2016) Preparation and characterization of silver nanoparticles and their use in catalytic reduction of 4-nitrophenol. WJNSE 6(1):29–37. https://doi.org/10.4236/wjnse.2016.61003

Almatroudi A, Khadri H, Azam M, Rahmani AH, Al Khaleefah FK, Khateef R, Allemailem KS (2020) Antibacterial, antibiofilm and anticancer activity of biologically synthesized silver nanoparticles using seed extract of *Nigella sativa*. Processes 8(4):388. https://doi.org/10.3390/pr8040388

Ansari M, Bhor D, Pai R, Sen D, Mazumder S, Ghosh K, Kolekar D, Ramana V (2017) Cobalt nanoparticles for biomedical applications: Facile synthesis, physiochemical characterization, cytotoxicity behavior and biocompatibility. Appl Surf Sci 414:171–187. https://doi.org/10.1016/j.apsusc.2017.03.002

Aouay M, Aguado RJ, Bayés G et al (2024) In-situ synthesis and binding of silver nanoparticles to dialdehyde and carboxylated cellulose nanofibrils, and active packaging therewith. Cellulose 31:5687–5706. https://doi.org/10.1007/s10570-024-05918-5

Aslam M, Fozia F, Gul A, Ahmad I, Ullah R, Bari A, Mothana A, Hussain H (2021) Phyto-extract-mediated synthesis of silver nanoparticles using aqueous extract of *Sanvitalia procumbens*, and characterization, optimization and photocatalytic degradation of azo dyes orange G and direct blue-15. Molecules 26(20):6144. https://doi.org/10.3390/molecules26206144

Awais S, Munir H, Najeeb J, Anjum F, Naseem K, Kausar N, Najeeb N (2023) Green synthesis of iron oxide nanoparticles using *Bombax malabaricum* for antioxidant, antimicrobial and photocatalytic applications. J Clean Prod 406:136916. https://doi.org/10.3390/nano13222919

Bhavi SM, Mirji SK, Thokchom B, Singh SR, Maliger RB, Bhat SS, Jadidi SA (2024) Potential antidiabetic properties of Syzygium Cumini (L.) Skeels leaf extract-mediated silver nanoparticles. Austin J Anal Pharm Chem 11(1):1168. https://doi.org/10.26420/austinjanalpharmchem.2024.1168

Bhavi SM, Padti AC, Thokchom B, Singh SR, Bhat SS, Bajire SK, Yarajarla RB (2024b) Biogenic silver nanoparticles from *Simarouba glauca* DC leaf extract: synthesis, characterization, and anticancer efficacy in lung cancer cells with protective effects in *Caenorhabditis elegans*. Nano

TransMed 3:100052. https://doi.org/10.1016/j.ntm.2024.100052

Bhavi SM, Thokchom B, Abbigeri MB, Bhat SS, Singh SR, Joshi P, Yarajarla RB (2024c) Green synthesis, characterization, antidiabetic, antioxidant and antibacterial applications of silver nanoparticles from *Syzygium caryophyllatum* (L.) Alston leaves. Process Biochem 145:89–103

Bhavi SM, Thokchom B, Singh SR, Bajire SK, Shastry RP, Srinath BS, Yarajarla RB (2025) *Syzygium malaccense* leaf extract-mediated silver nanoparticles: synthesis, characterization, and biomedical evaluation in *Caenorhabditis elegans* and lung cancer cell line. Green Chem Lett Rev 18(1):2456624. https://doi.org/10.1080/17518253.2025.2456624

Bohnert J, Shen B (1998) Transformation and compatible solutes. Sci Hortic (Amsterdam) 78(1–4):237–260. https://doi.org/10.1016/s0304-4238(98)00195-2

Bouftira I, Abdelly C, Sfar S (2008) Characterization of cosmetic cream with *Mesembryanthemum crystallinum* plant extract: influence of formulation composition on physical stability and antioxidant activity. Int J Cosmet Sci 30(6):443–452. https://doi.org/10.1111/j.1468-2494.2008.00469.x

MMCalvo ABMartín-Diana DRico MELópez-Caballero ÓMartínez-Álvarez 2022 Antioxidant, antihypertensive, hypoglycaemic and nootropic activity of a polyphenolic extract from the halophyte ice plant (*Mesembryanthemum crystallinum*) Foods 10.3390/foods11111581 Calvo MM, Martín-Diana AB, Rico D, López-Caballero ME, Martínez-Álvarez Ó (2022) Antioxidant, antihypertensive, hypoglycaemic and nootropic activity of a polyphenolic extract from the halophyte ice plant (*Mesembryanthemum crystallinum*). Foods. https://doi.org/10.3390/foods11111581

Cardoza JV, Ali Z, Simon S, Thakkar D, George SS, Isaac SP, George SS (2024) The Role of nanoparticles in accelerating tissue recovery and inflammation control in physiotherapy practices. Cureus. https://doi.org/10.7759/cureus.73540

Carreño A, Alberto P, de Souza M, de Mello L, Henriques A, Anastacio Alves L (2021) Considerations and technical pitfalls in the employment of the MTT assay to evaluate photosensitizers for photodynamic therapy. J Appl Sci 11(6):2603. https://doi.org/10.3390/app11062603

Castillo-Pérez LJ, Alonso-Castro AJ, Torres-Rico D, Acosta-Mata C, Barragan-Galvez JC, González-Rivera ML, Carranza-Álvarez C (2025) Catasetum integerrimum Hook (Orchidaceae) pseudobulbs ethanol extract induces antidiarrheal and antinociceptive actions. Chem Biodivers. https://doi.org/10.1002/cbdv.202403464

Chakraborty N, Banerjee J, Chakraborty P, Banerjee A, Chanda S, Ray K, Acharya K, Sarkar J (2022) Green synthesis of copper/copper oxide nanoparticles and their applications: a review. Green Chem Lett Rev 15(1):185–213. https://doi.org/10.1080/17518253.2022.2025916

Chandrasekharan S, Chinnasamy G, Bhatnagar S (2022) Sustainable phyto-fabrication of silver nanoparticles using *Gmelina arborea* exhibit antimicrobial and biofilm inhibition activity. Sci Rep 12:1–156. https://doi.org/10.1038/s41598-021-04025-w

Chelliah P, Wabaidur SM, Sharma HP, Jweeg MJ, Majdi HS, AL.Kubaisy MMR, Lai WC (2023) Green synthesis and characterizations of cobalt oxide nanoparticles and their coherent photocatalytic and antibacterial investigations. Water 15(5):910. https://doi.org/10.3390/w15050910

Das E, Abu-Yousef A, Majdalawieh F, Narasimhan S, Poltronieri P (2020) Green synthesis of encapsulated copper nanoparticles using a hydroalcoholic extract of *Moringa oleifera* leaves and assessment of their antioxidant and antimicrobial activities. Molecules 25(3):555. https://doi.org/10.3390/molecules25030555

Delattre C, Fenoradosoa A, Michaud P (2011) Galactans: an overview of their most important sourcing and applications as natural polysaccharides. Braz Arch Biol Techn 54:1075–1092. https://doi.org/10.1590/S1516-89132011000600002

Domingues SZ, Timmers LFSM, Granada CE (2022) Cellulase production by bacteria is a strain-specific characteristic with a high biotechnological potential. A review of cellulosome of highly studied strains. Cellulose 29:8065–8083. https://doi.org/10.1007/s10570-022-04790-5

El-Bisi MK, El-Rafie HM, El-Rafie MH, Hebeish A (2013) Honeybee for eco-friendly green synthesis of silver nanoparticles and application to cotton textile. Egypt J Chem 56(3):187–198. https://doi.org/10.21608/EJCHEM.2013.1107

El-Rafie H, El-Rafie M, AbdElsalam H, El-Sayed W (2016a) Antibacterial and anti-inflammatory finishing of cotton by microencapsulation using three marine organisms. Int J Biol Macromol 86:59–64. https://doi.org/10.1016/j.ijbiomac.2016.01.039

El-Rafie M, Abd El-Aziz M, Zahran K (2016b) Bioactivities of gold and iron oxide nanoparticles biosynthesized from the edible plant *Corchorus olitorius*. Pharm Lett 8(19):156–164

El-Rafie M, Zahran K, Raoof A (2022) Cotton bandages finished with microcapsules of volatile organic constituents of marine macro-algae for wound healing. Bioprocess Biosyst Eng 45(1):203–216. https://doi.org/10.1007/s00449-021-02653-0

El-Rafie M, El-Aziz A, Zahran K (2023) In vitro cytotoxicity against breast cancer using biogenically synthesized gold and iron oxide nanoparticles derived from the hydroethanolic extract of *Salvia officinalis L.* Chem Pap 77:361–373. https://doi.org/10.1007/s11696-022-02464-x

El-Sayyad S, Abdel Maksoud A, Fahim A et al (2022) Gamma radiation induced synthesis of gold/bioactive glass nanocomposite for promising antimicrobial, and antibiofilm activities. J Clust Sci 34:1877–1891. https://doi.org/10.1007/s10876-022-02357-9

Faisal S, Jan H, Abdullah Alam M, Hussain Z, Km Sultana, Ali Z, Uddin M (2022) In vivo analgesic anti-inflammatory, and anti-diabetic screening of bacopa monnieri-synth esized copper oxide nanoparticles 131 S. ACS Omega 7(5):4071–4082. https://doi.org/10.1021/acsomega.1c05410

Ganesan K, Jothi K, Natarajan A, Rajaram A, Ravichandran S, Ramalingam S (2020) Green synthesis of copper oxide nanoparticles decorated with graphene oxide for anticancer activity and catalytic applications. Arab J Chem

13(8):6802–6814. https://doi.org/10.1016/j.arabjc.2020.06.033

Giri K, Jena B, Biswal B, Pradhan K, Arakha M, Acharya S, Acharya L (2022) Green synthesis and characterization of silver nanoparticles using *Eugenia roxburghii* DC. extract and activity against biofilm-producing bacteria. Sci Rep 12(1):8383. https://doi.org/10.1038/s41598-022-12484-y

Gomez-Hermoso-de-Mendoza J, Gutierrez J, Tercjak A (2023) Highly hydrophobic cellulose acetate mats modified with poly (ethylene oxide-b-propylene oxide-b-ethylene oxide) triblock copolymer and TiO2 nanoparticles by electrospinning. Cellulose 30:9501–9515. https://doi.org/10.1007/s10570-023-05417-z

Hafeez M, Shaheen R, Akram B, Zainul A, Haq S, Mahsud S, Ali S, Khan T (2020) Green synthesis of cobalt oxide nanoparticles for potential biological applications. Mater Res Express 7(2):025019. https://doi.org/10.1088/2053-1591/ab70dd

He B, Ai J, Ren J et al (2022) Alkyl ketene dimer grafted cationic cellulose stabilizing nano magnesium oxide for efficient protection of acidic paper. Cellulose 29(16):8863–8877. https://doi.org/10.1007/s10570-022-04812-2

Hebeish A, El-Naggar E, Fouda G, Ramadan A, Al-Deyab S, El-Rafie H (2011) Highly effective antibacterial textiles containing green synthesized silver nanoparticles. Carbohydr Polym 86(2):936–940. https://doi.org/10.1016/j.carbpol.2011.05.048

Huq MA (2020) Green synthesis of silver nanoparticles using *Pseudoduganella eburnea* MAHUQ-39 and their antimicrobial mechanisms investigation against drug resistant human pathogens. Int J Mol Sci 21(4):1510. https://doi.org/10.3390/ijms21041510

Ibrahim SS, Al-darwesh MY, Arkawazi SW, Babakr KA, Qader IN (2025) Synthesis, characterization, antioxidant, antibacterial activity, and molecular docking studies of Zn (II) and Cu (II) complexes nanoparticles. J Mol Struct 1326:141120. https://doi.org/10.1016/j.inoche.2024.113304

Ibtissem B, Abdelly C, Sfar S (2012) Antioxidant and antibacterial properties of *Mesembryanthemum crystallinum* and *Carpobrotus edulis* extracts. Adv Chem Eng Sci 2:359–365. https://doi.org/10.4236/aces.2012.23042

Ihsan S, Munir H, Meng Z, Tayyab M, Zeeshan N, Rehman A, Irfan M (2024) Tragacanth gum-based copper oxide nanoparticles: comprehensive characterization, antibiofilm, antimicrobial and photocatalytic potentials. Int J Biol Macromol 268:131600. https://doi.org/10.1016/j.ijbiomac.2024.131600

Irfan M, Munir H, Ismail H (2021) Moringa oleifera gum-based silver and zinc oxide nanoparticles: green synthesis, characterization and their antibacterial potential against MRSA. Biomater Res 25:17. https://doi.org/10.1186/s40824-021-00219-5

Irfan M, Munir H, Ismail H (2022) Characterization and fabrication of zinc oxide nanoparticles by gum Acacia modesta through green chemistry and impregnation on surgical sutures to boost up the wound healing process. Int J Biol Macromol 204:466–475. https://doi.org/10.1016/j.ijbiomac.2022.02.043

Jadhav H, Pisal B, Chavan R, Patil M, Patil B, Pagare K (2021) Electrochemical supercapacitive performance study of spray pyrolyzed cobalt oxide film. Mater Today Proc 43:2742–2746. https://doi.org/10.1016/j.matpr.2020.06.477

Jan H, Zaman G, Usman H, Ansir R, Drouet S, Gigliolo-Guivarc'h N, Hano C, Abbasi H (2021) Biogenically proficient synthesis and characterization of silver nanoparticles (Ag-NPs) employing aqueous extract of *Aquilegia pubiflora* along with their in vitro antimicrobial, anti-cancer and other biological applications. JMR T 15:950–968. https://doi.org/10.1016/j.jmrt.2021.08.048

Kalaiselva V, Rajasekaran A (2009) Biosynthesis of silver nanoparticles from *Aspergillus niger* and evaluation of its wound healing activity in experimental rat model. Int J Pharm Tech Res 4:152

Kang W, Joo M (2023) Comparative analysis on phytochemical properties, anti-oxidative, and anti-inflammatory activities of the different organs of the common ice plant *Mesembryanthemum crystallinum L.* Appl Sci 13(4):2527. https://doi.org/10.3390/app13042527

Kenawy ER, El-Meligy M, Ghaly Z et al (2024) Novel physically crosslinked caffeine and vitamin C-loaded PVA/Aloe vera hydrogel membranes for topical wound healing: synthesis, characterization and in-vivo wound healing tests. J Polym Environ 32:2140–2157. https://doi.org/10.1007/s10924-023-03083-7

Khanal N, Sharma R, Paudyal H, Parajuli K, Dahal B, Ganga C, Kalauni K (2022) Green synthesis of silver nanoparticles from root extracts of Rubus ellipticus Sm and comparison of antioxidant and antibacterial activity. J Nanomater 1:832587. https://doi.org/10.1155/2022/1832587

Khani R, Irani M (2020) A reusable reduced graphene oxide-cobalt oxide nanocomposite with excellent yield as adsorbent for determination trace-level of brilliant green in environmental water samples. Res Chem Intermed 46(4):2137–2154. https://doi.org/10.1007/s11164-020-04083-1

Khorrami S, Zarrabi A, Khaleghi M, Danaei M, Mozafari M (2018) Selective cytotoxicity of green synthesized silver nanoparticles against the MCF-7 tumor cell line and their enhanced antioxidant and antimicrobial properties. Int J Nanomed 13:8013. https://doi.org/10.2147/IJN.S189295

Kir I, Mohammed H, Laouini S et al (2024) Plant extract-mediated synthesis of CuO nanoparticles from lemon peel extract and their modification with polyethylene glycol for enhancing photocatalytic and antioxidant activities. J Polym Environ 32:718–734. https://doi.org/10.1007/s10924-023-02976-x

Kolahalam LA, Prasad KRS, Krishna PM, Supraja N (2024) *Lawsonia inermis* plant-based cobalt oxide nanoparticles: synthesis, characterization and their biological studies. Results Chem 7:101367. https://doi.org/10.1016/j.rechem.2024.101367

Koyyati R, Kudle R, Padigya M (2016) Evaluation of antibacterial and cytotoxic activity of green synthesized cobalt nanoparticles using *Raphanus sativus* var. *longipinnatus* leaf extract. Int J PharmTech Res 9(3):466–472

Krishnan D, Durai D, Kabanov D, Hosnedlova B, Kepinska M, Fernandez C, Ruttkay B, Gunug V, Farid A (2020)

Silver nanomaterials for wound dressing applications. J Pharm 2(9):821. https://doi.org/10.3390/pharmaceutics12090821

Lakshmi A, Venkata K, Anthony SP (2019) Synthesis of Solanum nigrum mediated copper oxide nanoparticles and their photocatalytic dye degradation studies. J Chem Technol Biotechnol 88:1971–1977. https://doi.org/10.1088/2053-1591/ab52a6

Li Y, Liu F, Fan Y, Cheng G, Song W, Zhou J (2018) Silver palladium bimetallic core-shell structure catalyst supported on TiO_2 for toluene oxidation. Appl Surf Sci 462:207–212. https://doi.org/10.1016/j.apsusc.2018.08.023

Loconsole D, Murillo-Amador B, Cristiano G, de Lucía B (2019) Halophyte common ice plants: a future solution to arable land salinization. Sustainability. https://doi.org/10.3390/su11216076

Masri A, Anwar A, Ahmed D, Siddiqui B, Raza M, Khan A (2018) Silver nanoparticle conjugation-enhanced antibacterial efficacy of clinically approved drugs cephradine and vildagliptin. Antibiotics 7(4):100. https://doi.org/10.3390/antibiotics7040100

Masud S, Munir H, Irfan M, Tayyab M (2023) *Allium cepa*-based zinc oxide nanoparticles: characterization and biochemical potentials. Bioinspir Biomim Nanobiomater 12(2):82–93

Mukaratirwa-Muchanyereyi N, Gusha C, Mujuru M, Guyo U, Nyoni S (2022) Synthesis of silver nanoparticles using plant extracts from *Erythrina abyssinica* aerial parts and assessment of their anti-bacterial and antioxidant activities. Results Chem 4:100402. https://doi.org/10.1016/j.rechem.2022.100402

Naikoo GA, Bano M, Hassan IU, Ayyub MM, Zamani Pedram M (2023) Trimetallic CuO/Ag/NiO supported with silica nanoparticles based composite materials for green hydrogen production. Sci Rep 13(1):16909. https://doi.org/10.1038/s41598-023-43697-4

Narayana MSV, Rajesh N, Dastagiri C, Mobeen SA, Khadri H, Chandrasekhar T, Riazunnisa K (2024) Pleurotus ostreatus copper nanoparticles: In vitro and in silico evaluation of the antioxidant, antibacterial and antidiabetic activities. Chem Biodiv e202402361. https://doi.org/10.1002/cbdv.202403464

Okaiyeto K, Hoppe H, Okoh I (2021) Plant-based synthesis of silver nanoparticles using aqueous leaf extract of *Salvia officinalis*: characterization and its antiplasmodial activity. J Clust Sci 32(1):101–109. https://doi.org/10.1007/s10876-020-01766-y

Pandey C, Pandey G (2016) One-pot two-step rapid synthesis of 3-aminopropyltrimethoxysilane-mediated highly catalytic Ag@(PdAu) trimetallic nanoparticles. Catal Sci Technol 6(11):3911–3917. https://doi.org/10.3390/bios11040122

Parveen ST, Riazunnisa K (2025) Phytofabrication of copper nanoparticles using *Momordica cymbalaria* fruit extract and their antibacterial, antioxidant and anti-inflammatory properties. Hybrid Adv 9:100421. https://doi.org/10.1016/j.hybadv.2025.100421

Prabaharan M, Sadaiyandi K, Mahendran M, Sagadevan S (2017) Precipitation method and characterization of cobalt oxide nanoparticles. Appl Phys A 123:1–6. https://doi.org/10.1007/s00339-017-0786-8

Puntes F, Krishnan M, Alivisatos P (2001) Colloidal nanocrystal shape and size control: the case of cobalt. Science 291(5511):2115–2117. https://doi.org/10.1126/science.1057553

Rajeshkumar R, Pavadai P, Panneerselvam T et al (2024) Enhanced delivery of retinoic acid to breast cancer cells by folate receptor-targeted folic acid-conjugated glutenin nanoparticles for promising treatment of breast cancer. J Polym Environ 32:2120–2139. https://doi.org/10.1007/s10924-023-03107-2

Raji O, Eijsink VGH, Master E et al (2023) Modularity impacts cellulose surface oxidation by a lytic polysaccharide monooxygenase from *Streptomyces coelicolor*. Cellulose 30:10783–10794. https://doi.org/10.1007/s10570-023-05551-8

Ramaswamy P, Narendhran S, Sivaraj R (2016) Potentiating effect of ecofriendly synthesis of copper oxide nanoparticles using brown alga: antimicrobial and anticancer activities. Bull Mater Sci 39(2):361–364. https://doi.org/10.1007/s12034-016-1173-3

Rehan M, Mashaly HM, Abdel-Aziz MS et al (2024) Viscose fibers decorated with silver nanoparticles via an in-situ green route: UV protection, antioxidant activities, antimicrobial properties, and sensing response. Cellulose 31:5899–5930. https://doi.org/10.1007/s10570-024-05856-2

Rinaudo M (2014) Biomaterials based on a natural polysaccharide: alginate. TIP Revista Especializada En Ciencias Químico-Biológicas 17(1):92–96. https://doi.org/10.1016/S1405-888X(14)70322-5

Riss L, Moravec A, Niles L, Duellman S, Benink A, Worzella J, Minor L (2016) Cell viability assays. Assay Guidance Manual

Rostamitabar M, Ghahramani A, Seide G et al (2022) Drug loaded cellulose–chitosan aerogel microfibers for wound dressing applications. Cellulose 29:6261–6281. https://doi.org/10.1007/s10570-022-04630-6

Schiavi LSDO, Gonçalves MA, Delgado-Silva ADO et al (2024) Properties of fiber cement reinforced with cellulose pulp modified by plasma treatment with sulfur hexafluoride (SF6). Cellulose. https://doi.org/10.1007/s10570-024-05885-x

Sedighi A, Montazer M, Hemmatinejad, (2014) Copper nanoparticles on bleached cotton fabric: in situ synthesis and characterization. Cellulose 21(3):2119–2132. https://doi.org/10.1007/s10570-014-0215-5

Shafqat S, Munir H, Najeeb J, Naseem K, Irfan M (2025) Fabrication of multifaceted alpha-alumina nanoparticles: exploring bioactive and photocatalytic properties. BioNanoScience 15(2):1–16. https://doi.org/10.1007/s12668-025-01839-0

Sharaf S, Farouk A, El-Hady M (2016) Novel conductive textile fabric based on polyaniline and CuO nanoparticles. Int J PharmTech Res 9(6):461–472

Sharaf SS, El-Shafei AM, Refaie R et al (2022) Antibacterial and wound healing properties of cellulose acetate electrospun nanofibers loaded with bioactive glass nanoparticles; in-vivo study. Cellulose 29:4565–4577. https://doi.org/10.1007/s10570-022-04570-1

Siddiqui A, Alhadlaq A, Ahmad J, Al-Khedhairy A, Musarrat J, Ahamed M (2013) Copper oxide nanoparticles induced mitochondria mediated apoptosis in human hepatocarcinoma cells. PLoS ONE 8(8):e69534. https://doi.org/10.1371/journal.pone.0069534

Singh SR, Kittur B, Bhavi SM, Thokchom B, Padti AC, Bhat SS, Yarajarla RB (2025) The effect of *Clitoria ternatea* L. flowers-derived silver nanoparticles on A549 and L-132 human cell lines and their antibacterial efficacy in *Caenorhabditis elegans* in vivo. Hybrid Adv 8:100359. https://doi.org/10.1016/j.hybadv.2024.100359

Suresh S, Karthikeyan S, Jayamoorthy K (2016) FTIR and multivariate analysis to study the effect of bulk and nano copper oxide on peanut plant leaves. J Sci Adv Mater Devices 1(3):343–350. https://doi.org/10.1016/j.jsamd.2016.08.004

Tang R, Yan X, Hu J et al (2024) Carboxymethyl chitosan/alginate/polyethylene glycol composite hydrogel for nucleic acid lysis solution storage at the point of care. Cellulose. https://doi.org/10.1007/s10570-024-05889-7

Vanlalveni C, Lallianrawna S, Biswas A, Selvaraj M, Changmai B, Rokhum SL (2021) Green synthesis of silver nanoparticles using plant extracts and their antimicrobial activities: a review of recent literature. RSC Adv 11(5):2804–2837. https://doi.org/10.1039/d0ra09941d

Vasas A, Orbán-Gyapai O, Hohmann J (2015) The genus *Rumex*: review of traditional uses, phytochemistry and pharmacology. J Ethnopharmacol 175:198–228. https://doi.org/10.1016/j.jep.2015.09.001

Veerasamy R, Xin TZ, Gunasagaran S, Xiang TFW, Yang EFC, Jeyakumar N, Dhanaraj SA (2011) Biosynthesis of silver nanoparticles using mangosteen leaf extract and evaluation of their antimicrobial activities. J Saudi Chem Soc 15(2):113–120. https://doi.org/10.1016/j.jscs.2010.06.004

Waris A, Din M, Ali A, Afridi S, Baset A, Khan AU, Ali M (2021) Green fabrication of Co and Co3O4 nanoparticles and their biomedical applications: a review. Open Life Sci 16(1):14–30. https://doi.org/10.1515/biol-2021-0003

Xie H, Jin L, Morris A, Zha Q, Chen Q, Yi Y, Li E, Wang J, Gao J, Nie P, Shang P, Xie Y (2016) Advances on bioactive polysaccharides from medicinal plants. Crit Rev Food Sci Nutr 56(sup1):S60–S84. https://doi.org/10.1080/10408398.2015.1069255

Yapias R (2024) Phytoremediation and nutritional potential of the ice plants (Mesembryanthemum crystallinum L,). SABRAO J Breed Genets. https://doi.org/10.54910/sabrao2024.56.4.27

Yazdanshenas M, Shateri-Khalilabad M (2013) In situ synthesis of silver nanoparticles on alkali-treated cotton fabrics. J Ind Text 42(4):459–474. https://doi.org/10.1177/1528083712444297

Yedoti V, Supraja N (2024) A review on algal mediated synthesized metallic nanoparticles: an eco-friendly approach for sustainable nanotechnology. Curr j Appl Sci Technol. https://doi.org/10.9734/cjast/2024/v43i64381

Publisher's Note Springer Nature remains neutral with regard to jurisdictional claims in published maps and institutional affiliations.